Journal of Mathematical Modeling
Vol. 11, No. 3, 2023, pp. 547–572. Research Article

JMM

Semi-algebraic mode analysis for multigrid method on regular rectangular and triangular grids

Noora Habibi[†], **Ali Mesforush**[†*]

[†]*Faculty of Mathematical Sciences, Shahrood University of Technology, Shahrood, Iran*
Email(s): habibi85nu@gmail.com, ali.mesforush@shahroodut.ac.ir

Abstract. In this work, a Semi-Algebraic Mode Analysis (SAMA) technique for multigrid waveform relaxation method applied to the finite element discretization on rectangular and regular triangular grids in two dimensions and cubic and triangular prism elements in three dimensions for the heat equation is proposed. For all the studied cases especially for the general triangular prism element, both the stiffness and mass stencils are introduced comprehensively. Moreover, several numerical examples are included to illustrate the efficiency of the convergence estimates. Studying this analysis for the finite element method is more involved and more general than that finite-difference discretization since the mass matrix must be considered. The proposed analysis results are a very useful tool to study the behavior of the multigrid waveform relaxation method depending on the parameters of the problem.

Keywords: Finite element method, waveform relaxation method, multigrid technique, semi-algebraic mode analysis.
AMS Subject Classification 2010: 34A34, 65L05.

1 Introduction

Let us consider as a model problem, the heat equation with homogeneous Dirichlet boundary conditions [12, 14]

$$\begin{aligned} &D_t u(\mathbf{x},t) - \Delta u(\mathbf{x},t)) = f(\mathbf{x},t), \quad \mathbf{x} \in \Omega, \quad t > 0, \\ &u(\mathbf{x},t) = 0, \quad \text{on } \partial\Omega, \quad t > 0, \\ &u(\mathbf{x},0) = g(\mathbf{x}), \quad \mathbf{x} \in \Omega, \end{aligned} \tag{1}$$

where $\Omega \subset \mathbb{R}^d$, for $d = 2$ (or $d = 3$) is a bounded domain with boundary $\partial\Omega$. To establish the finite element approximation of our problem, let Ω_h be a triangulation of Ω, satisfying the usual admissibility

*Corresponding author
Received: 07 December 2022 / Revised: 02 Jun 2023/ Accepted: 26 Jun 2023
DOI: 10.22124/jmm.2023.23386.2086

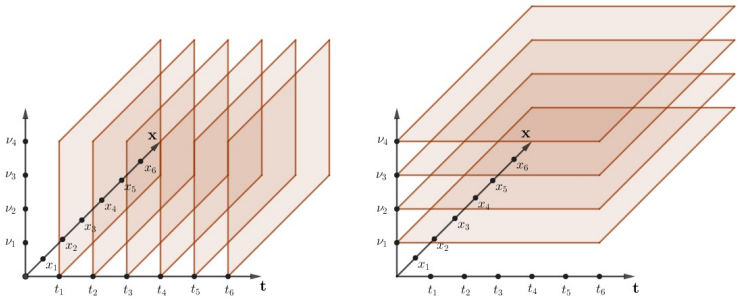

Figure 1: Time-stepping (left) versus waveform relaxation (right). In this figure ν_i, for $i = 1,2,\ldots$ indicates to the iterations of two methods.

assumption, i.e., the intersection of two different elements is either empty, a vertex, or a whole edge. Let V_h be the finite element space of continuous piecewise polynomials (of degree ≤ 3) associated with Ω_h vanishing on the boundary $\partial\Omega$. The discrete approximation $u_h \in V_h$ solves the following problem

$$(D_t u_h, v_h) + a(u_h, v_h) = (f, v_h), \quad v_h \in V_h,$$

where

$$(D_t u_h, v_h) = \int_\Omega (D_t u_h) v_h \, \mathrm{d}\mathbf{x}, \qquad (f, v_h) = \int_\Omega f v_h \, \mathrm{d}\mathbf{x},$$
$$a(u_h, v_h) = \int_\Omega \nabla u_h \cdot \nabla v_h \, \mathrm{d}\mathbf{x}.$$

Let $\{\phi_1, \ldots, \phi_N\}$ be the nodal basis of V_h, i.e., $\phi_i(\mathbf{x}_j) = \delta_{ij}$, with $\mathbf{x}_j$ an interior node of the mesh Ω_h. The approximation $u_h = \sum_{i=1}^N u_i(t)\phi_i(\mathbf{x})$, is found by solving the following set of equations,

$$(D_t u_h, \phi_j) + a(u_h, \phi_j) = (f, \phi_j), \quad \text{for } j = 1,2,\ldots,N.$$

We rewrite these equations in terms of the mass matrix $B_h = \{(\phi_i, \phi_j)\}$ and the stiffness matrix $A_h = \{a(\phi_i, \phi_j)\}$, in a more standard form, as a system of ordinary differential equations (ODEs)

$$B_h \dot{\mathbf{u}}_h(t) + A_h \mathbf{u}_h(t) = \mathbf{F}_h(t), \quad \mathbf{u}_h(0) = g_h, \quad t > 0, \tag{2}$$

where $\mathbf{u}_h(t) = [u_1(t), u_2(t), \ldots, u_N(t)]^t \in \mathbb{R}^N$ and the coefficient matrices $A_h, B_h \in \mathbb{R}^{N\times N}$ and the right hand side $\mathbf{F}_h(t) = [(f,\phi_1), (f,\phi_2), \ldots, (f,\phi_N)]^t \in \mathbb{R}^N$ are considered.

We have many choices to pick a suitable method for solving the obtained ODE system (2). In general, we can divide all the well-known methods into two classes: time-marching approaches and, time-parallel techniques. In a time marching approach, we solve in each time step a time-independent problem and we then go to the next time step. Indeed, as we can get out from its name, each time step will be solved after the other in a sequential manner, see Figure 1 (left). Although this approach is simple when we need multiprocessing capability or parallelization of the temporal variable we have to seek another approach. So we consider a full space-time method. The time parallel class itself can be classified into four groups of methods, see [10]: multiple shooting; domain decomposition and waveform

relaxation; space-time multigrid method; and direct time parallel methods. Here, we only concentrate on the waveform relaxation method and in particular, on its multigrid extension.

The waveform relaxation method (WR) is a technique for solving ordinary differential equations. It can be also applied to time-dependent PDEs where their spatial derivative is replaced by a discrete formula (obtained by the finite element method in our particular case) as a viewpoint of the method of lines scheme. The WR method is based on splitting matrices A_h and B_h as $B_h = M_{B_h} - N_{B_h}$ and $A_h = M_{A_h} - N_{A_h}$, leading to the following iteration

$$M_{B_h}\dot{\mathbf{u}}_h^k(t) + M_{A_h}\mathbf{u}_h^k(t) = N_{B_h}\dot{\mathbf{u}}_h^{k-1}(t) + N_{A_h}\mathbf{u}_h^{k-1}(t) + F_h(t), \tag{3}$$

where $\mathbf{u}_h^k(0) = g_h$, for $k \geq 1$ and $\mathbf{u}_h^k(t)$ indicates the approximation of $\mathbf{u}(t)$ at iteration k. It is natural to define $\mathbf{u}_h^0(t)$ along the whole time interval equal to the initial condition, i.e $\mathbf{u}_h^0(t) = g_h,\ t > 0$. Considering the decomposition of matrices A_h and B_h as $A_h = -L_{A_h} + D_{A_h} - U_{A_h}$ and $B_h = -L_{B_h} + D_{B_h} - U_{B_h}$, where L_{A_h}, L_{B_h} are strictly lower triangular matrices, D_{A_h}, D_{B_h} are diagonal matrices, and U_{A_h}, U_{B_h} are strictly upper triangular matrices, for the Gauss-Seidel waveform relaxation method, which is considered in this work, the splittings in (3) are as follows

$$\begin{aligned} M_{A_h} &= -L_{A_h} + D_{A_h}, \quad N_{A_h} = U_{A_h}, \\ M_{B_h} &= -L_{B_h} + D_{B_h}, \quad N_{B_h} = U_{B_h}. \end{aligned}$$

We use the multigrid technique to accelerate the convergence of the Gauss-Seidel waveform relaxation method. A multigrid acceleration of this method was firstly studied in [8] and independently developed in [13].

In order to apply a geometric multigrid waveform relaxation procedure, the coarsening applies only in the spatial domain (semi-coarsening in space) and we consider a hierarchy of grids like $\Omega_{2^l h} \subset \ldots \subset \Omega_{2h} \subset \Omega_h$. We obtain a new iterate $\mathbf{u}_h^k$ from the former waveform $\mathbf{u}_h^{k-1}$ in three steps: Pre-smoothing, coarse grid correction, and post smoothing. In Algorithm 1 we present the multigrid waveform relaxation algorithm (WRMG) depending on the defined waveform relaxation method as smoother and the rest of the operators involved in the multigrid procedure. We consider standard coarsening for constructing the coarse meshes and discretization coarse grid approximation (DCA) in coarser grids. Regarding intergrid transfer operators, the interpolation operators, are the nine points and seven points stencil operators corresponding to the bilinear and linear interpolations, respectively for two-dimensional problems. Their generalization for three-dimensional problems respectively are the trilinear and non-symmetric bilinear interpolation operators defined on corresponding cubic and triangular prism elements. The restriction operators are considered as the adjoint of the prolongation operators.

In Algorithm 1, using the Crank-Nicolson approach for time discretization we obtain a space-time multigrid method with coarsening only in space. Thus, we have time-line Gauss-Seidel waveform relaxation, with standard full weighting restriction and linear interpolation in space for data transfer between the levels in the multigrid hierarchy.

We analyze the convergence factor of the multigrid waveform relaxation method by Semi-Algebraic Mode Analysis (SAMA). This analysis was introduced by [2] for predicting the convergence factor of time-dependent Partial Differential Equations (PDEs) which is a generalization for Local Fourier Analysis (LFA). The LFA is the most powerful technique for predicting the convergence of multigrid methods, [12, 14]. This method analyzes the behavior of the local components involved in multigrid methods on a basis of complex exponential functions. LFA, however, has not been successful in predicting the

Algorithm 1 Multigrid waveform relaxation based on Gauss-Seidel smoother $\mathbf{u}_h^k(t) \rightarrow \mathbf{u}_h^{k+1}(t)$.

if we are on the coarsest grid (given by spatial grid size $2^l h = h_0$), then solve
the following equation by a direct or fast solver **then**
$$B_{h_0}\dot{\mathbf{u}}_{h_0}^{k+1}(t) + A_{h_0}\mathbf{u}_{h_0}^{k+1}(t) = F_{h_0}(t).$$
else
(*Coarse grid correction*)
Compute the defect $\bar{d}_h^k(t) = F_h(t) - B_h\dot{v}_h^k(t) - A_h v_h^k(t)$.
Restrict the defect $\bar{d}_{2h}^k(t) = I_h^{2h}\bar{d}_h^k(t)$.
Perform $\gamma \geq 1$ cycles of WRMG on Ω_{2h} to solve the following defect equation,
$B_{2h}\dot{e}_{2h}^k(t) + A_{2h}e_{2h}^k(t) = \bar{d}_{2h}^k(t)$, $e_{2h}^k(0) = 0$.
Interpolate the correction $e_h^k(t) = I_{2h}^h e_{2h}^k(t)$.
Correct the current approximation with the interpolation of the correction,
$v_h^{k+1}(t) = v_h^k(t) + e_h^k(t)$.
(*Postsmoothing*)
Perform k_2 steps of Gauss-Seidel waveform relaxation, $\mathbf{u}_h^{k+1}(t) = S^{k_2}\left(v_h^{k+1}(t)\right)$.
end if

convergence factor for time-dependent PDE problems, [2, 3]. So, we utilize SAMA to analyze the convergence factor of multigrid waveform relaxation on the considered heat equation, in this work. The main idea of SAMA is a combination of LFA with algebraic computation for the non-local part, which is the time variable here.

The remainder of this paper is organized as follows. First, in Subsections 2.3-2.5, we explain the two-grid SAMA analysis in two dimensions on the rectangular and triangular meshes where the Gauss-Seidel waveform relaxation with multigrid acceleration is considered. In the rest of section 2, Subsections 2.6 and 2.7, we will present our analysis for the model problem (1) on the two different domains, a square, and a parallelogram, obtaining all required stencils involved in the finite element method with linear and bilinear basis functions. The extension of SAMA analysis to three dimensions is performed assuming cubic and triangular prism meshes. Again in this section, The required stencils are computed especially on the general triangular prism element that is new. After that, we illustrate the efficiency of the two-grid SAMA analysis as a prediction of a W-cycle multigrid waveform relaxation, in Section 3. Conclusions are drawn in Section 4.

2 Semi-algebraic mode analysis in two dimension

Now, we describe the convergence analysis of the multigrid waveform relaxation method by SAMA based on the finite element method considering bilinear and linear basis functions. First, we explain general components corresponding to each case, and then we follow the analysis with the same consideration for both rectangular and triangular grids. All that we need to do are depicted in the following steps:

1. First, we present some primary definitions for both rectangular and triangular grids,
2. Next, we explain SAMA smoothing analysis for the Gauss-Seidel relaxation procedure,
3. Then, we investigate the analysis for the coarse-grid correction operator,

4. Finally, we combine the two last steps to perform a complete two-grid analysis.

2.1 General definitions for rectangular elements.

We define the rectangular infinite grid

$$\mathscr{Q}_h = \{\mathbf{x} = \mathbf{kh} = (k_1 h_1, k_2 h_2),\ \mathbf{k} \in \mathbb{Z}^2\},$$

and the so-called Fourier modes as $\varphi_h(\boldsymbol{\theta}, \mathbf{x}) = e^{i\boldsymbol{\theta}\cdot\mathbf{x}} = e^{i\theta_1 x_1} e^{\theta_2 x_2}$ where $\mathbf{h}$ is the spatial discretization step and $\boldsymbol{\theta} \in \Theta_h = (-\pi/h, \pi/h]^2$. Now, we can define any discrete grid function for a fixed t on a formal linear combination of the Fourier modes by

$$u_h(\mathbf{x}, t) = \sum_{\boldsymbol{\theta}\in\Theta_h} c_{\boldsymbol{\theta}}(t)\varphi(\boldsymbol{\theta}, \mathbf{x}), \quad \mathbf{x} \in \mathscr{Q}_h, \tag{4}$$

where coefficients $c_{\boldsymbol{\theta}}(t)$ depend on the time variable. The Fourier modes yield the so-called Fourier space $\mathscr{F}(\mathscr{Q}_h) = \{\varphi_h(\boldsymbol{\theta}, \mathbf{x}),\ \boldsymbol{\theta} \in \Theta_h\}$, and they are formal eigenfunctions of any discrete operator L_h, e.g. for the standard discrete Laplace operator, $L_h = -\Delta_h = \frac{1}{h^2}[-1\ 2\ -1]$, the expression $L_h\varphi_h(\boldsymbol{\theta}, \mathbf{x}) = \widehat{L}_h(\boldsymbol{\theta})\varphi_h(\boldsymbol{\theta}, \mathbf{x})$ holds where

$$\widehat{L}_h(\boldsymbol{\theta}) = \frac{2}{h^2}\left(1 - \cos(\theta h)\right),$$

is the Fourier representation of L_h on the Fourier space, also called formal eigenvalue or the Fourier symbol of L_h.

We consider $\Theta_{2h} = (-\pi/2h, \pi/2h]^2$ and $\Theta_h \setminus \Theta_{2h}$ as the low- and high-frequency spaces, respectively. Here, we have used the standard coarsening which means that the step size is double on the coarse grid, denoted by $\mathscr{Q}_{2h}$.

2.2 General definitions for triangular elements.

LFA has been extended to multigrid methods for discretization on regular nonrectangular grids, see [4]. Here, we present some definitions to extend LFA to SAMA for PDE problems on regular triangular grids. The key issue is introducing the two-dimensional Fourier transform using coordinates in nonorthogonal bases.

Let $\{\mathbf{e}_1', \mathbf{e}_2'\}$ be a unitary basis of $\mathbb{R}^2$, $0 < \gamma < \pi$ the angle between the vectors of the basis, and $\{\mathbf{e}_1'', \mathbf{e}_2''\}$ its reciprocal basis; i.e., $\mathbf{e}_i' \cdot \mathbf{e}_j'' = \delta_{ij}$, $i, j = 1, 2$, where δ_{ij} is Kronecker's delta, see Figure 2. We denote by $y = (y_1, y_2)$, $y' = (y_1', y_2')$ and $y'' = (y_1'', y_2'')$ the coordinates of a point in the bases $\{\mathbf{e}_1, \mathbf{e}_2\}$, $\{\mathbf{e}_1', \mathbf{e}_2'\}$ and $\{\mathbf{e}_1'', \mathbf{e}_2''\}$, respectively where $\{\mathbf{e}_1, \mathbf{e}_2\}$ is the canonical basis. Since the new bases are reciprocal bases, by considering variable changes $\mathbf{x} = \mathrm{F}(\mathbf{x}')$ and $\boldsymbol{\theta} = \mathrm{G}(\boldsymbol{\theta}'')$ and applying them on usual Fourier transform and Fourier inversion formula, we can obtain the following expression for inner product in the new bases

$$\mathrm{G}(\boldsymbol{\theta}'') \cdot \mathrm{F}(\mathbf{x}') = \boldsymbol{\theta} \cdot \mathbf{x} = \theta_1'' x_1' + \theta_2'' x_2' = \boldsymbol{\theta}'' \cdot \mathbf{x}'.$$

A uniform triangular infinite grid oriented in the directions $\mathbf{e}_1'$ and $\mathbf{e}_2'$ is defined as

$$\mathscr{G}_h = \{\mathbf{x}' = (x_1', x_2') | x_i' = k_i h_i, k_i \in \mathbb{Z}, i = 1, 2\},$$

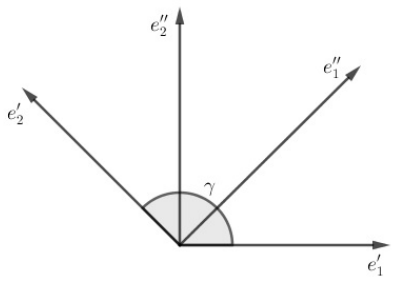

Figure 2: Reciprocal bases in $\mathbb{R}^2$.

where $\mathbf{h} = (h_1, h_2)$. A typical point in $\mathscr{G}_h$ is given by $x_1'\mathbf{e}_1' + x_2'\mathbf{e}_2'$, where $\mathbf{e}_1'$ and $\mathbf{e}_2'$ are unit vectors indicating the direction of two edges of the coarsest triangle, $\mathscr{T}$. Neglecting the boundary conditions of the discretized domain, $\mathscr{T}_h$, the discrete problem can be extended to the whole grid $\mathscr{G}_h$.

By considering the discrete Fourier transform of a grid function, we can define the Fourier modes $\varphi_h(\boldsymbol{\theta}'', \mathbf{x}') = \mathrm{e}^{i\theta_1'' x_1'} \mathrm{e}^{i\theta_2'' x_2'}$ and Fourier space $\mathscr{F}(\mathscr{G}_h) = \{\varphi_h(\boldsymbol{\theta}'', \cdot), \boldsymbol{\theta}'' \in \Theta_h''\}$, where $\boldsymbol{\theta}'' = (\theta_1'', \theta_2'') \in \Theta_h'' = (-\pi/h_1, \pi/h_1] \times (-\pi/h_2, \pi/h_2]$. As the rectangular grid case, any discrete grid function defined on $\mathscr{G}_h$ for a fixed t can be written as a formal linear combination of the Fourier modes, that is

$$u_h(\mathbf{x}, t) = \sum_{\boldsymbol{\theta}'' \in \Theta_h''} d_{\boldsymbol{\theta}''}(t) \varphi(\boldsymbol{\theta}'', \mathbf{x}'), \quad \mathbf{x}' \in \mathscr{G}_h, \tag{5}$$

where coefficients $d_{\boldsymbol{\theta}}(t)$ depend on the time variable.

Considering standard coarsening, the infinite coarse grid is

$$\mathscr{G}_{2h} = \{\mathbf{x}' = (x_1', x_2') | x_i' = 2k_i h_i, k_i \in \mathbb{Z}, i = 1, 2\}.$$

Moreover, $\Theta_{2h}'' = (-\pi/2h_1, \pi/2h_1] \times (-\pi/2h_2, \pi/2h_2]$ and $\Theta_h'' \setminus \Theta_{2h}''$ indicate respectively to the low- and high-frequency spaces.

We notice that SAMA on rectangular and nonrectangular grids can be performed similarly due to the fact that in the nonrectangular grid the grids and the frequency space are referred to as reciprocal bases, and the Fourier modes are in terms of $\boldsymbol{\theta}''$ and $\mathbf{x}'$. So in the rest of this part, we consider the unique notations $\mathbf{x} = (x_1, x_2)$ and $\boldsymbol{\theta} = (\theta_1, \theta_2)$. Furthermore, to perform a complete analysis on the triangular mesh one can substitute $\mathscr{Q}_h$, Θ_h and $c_{\boldsymbol{\theta}}$ respectively by $\mathscr{G}_h$, Θ_h'', and $d_{\boldsymbol{\theta}''}$.

2.3 Smoothing analysis

We describe the semi-algebraic smoothing analysis for the Gauss-Seidel waveform relaxation considering the spatial discrete operators B_h and A_h as $B_h = M_{B_h} - N_{B_h}$ and $A_h = M_{A_h} - N_{A_h}$, respectively that have been defined in section 1. We can write an iteration of the waveform relaxation method for the error grid function as

$$M_{B_h} \dot{e}_h^k(\mathbf{x}, t) + M_{A_h} e_h^k(\mathbf{x}, t) = N_{B_h} \dot{e}_h^{k-1}(\mathbf{x}, t) + N_{A_h} e_h^{k-1}(\mathbf{x}, t), \tag{6}$$

for $k \geq 1$, $\mathbf{x} \in \mathscr{Q}_{\mathbf{h}}$ and $t > 0$, where, $e_h^{k-1}(\cdot, t)$ and $e_h^k(\cdot, t)$ are the error grid functions at the $k-1$ and k iterations and $e_h^k(\mathbf{x}, 0) = 0$.

Following Eq. (4), we can write $e_h^i(\mathbf{x},t)$ in the ith iteration as

$$e_h^i(\mathbf{x},t)=\sum_{\boldsymbol{\theta}\in\Theta_h} c_{\boldsymbol{\theta}}^i(t)\varphi(\boldsymbol{\theta},\mathbf{x}),\quad \mathbf{x}\in\mathscr{Q}_h,\ t>0. \tag{7}$$

We denote as $\widehat{M}_{A_h}(\boldsymbol{\theta})$, $\widehat{M}_{B_h}(\boldsymbol{\theta})$, $\widehat{N}_{A_h}(\boldsymbol{\theta})$ and $\widehat{N}_{B_h}(\boldsymbol{\theta})$ the symbols of M_{A_h}, M_{B_h}, N_{A_h} and N_{B_h}, respectively. So, for each frequency $\boldsymbol{\theta}\in\Theta_h$ we have

$$\widehat{M}_{B_h}(\boldsymbol{\theta})\dot{c}_{\boldsymbol{\theta}}^k(t)+\widehat{M}_{A_h}(\boldsymbol{\theta})c_{\boldsymbol{\theta}}^k(t)=\widehat{N}_{B_h}(\boldsymbol{\theta})\dot{c}_{\boldsymbol{\theta}}^{k-1}(t)+\widehat{N}_{A_h}(\boldsymbol{\theta})c_{\boldsymbol{\theta}}^{k-1}(t), \tag{8}$$

for $k\geq 1$, $t>0$. Now, we apply the Crank-Nicolson time discretization to Eq. (8), obtaining a system of equations for $i=1,2,\ldots,M$,

$$\begin{aligned}&\widehat{M}_{B_h}(\boldsymbol{\theta})\frac{c_{\boldsymbol{\theta},i}^k-c_{\boldsymbol{\theta},i-1}^k}{\tau}-\widehat{N}_{B_h}(\boldsymbol{\theta})\frac{c_{\boldsymbol{\theta},i}^{k-1}-c_{\boldsymbol{\theta},i-1}^{k-1}}{\tau}\\&\quad=\frac{1}{2}\left(-\widehat{M}_{A_h}(\boldsymbol{\theta})c_{\boldsymbol{\theta},i}^k+\widehat{N}_{A_h}(\boldsymbol{\theta})c_{\boldsymbol{\theta},i}^{k-1}\right)+\frac{1}{2}\left(-\widehat{M}_{A_h}(\boldsymbol{\theta})c_{\boldsymbol{\theta},i-1}^k+\widehat{N}_{A_h}(\boldsymbol{\theta})c_{\boldsymbol{\theta},i-1}^{k-1}\right).\end{aligned} \tag{9}$$

where $c_{\boldsymbol{\theta},0}^k, c_{\boldsymbol{\theta},i}^0$ represents the initial condition $g(x)$. Thus, we can obtain its matrix form immediately,

$$\begin{bmatrix}c_{\boldsymbol{\theta},1}^k\\c_{\boldsymbol{\theta},2}^k\\\vdots\\c_{\boldsymbol{\theta},M}^k\end{bmatrix}=\widetilde{\mathscr{M}}_{h,\tau}^{-1}(\boldsymbol{\theta})\widetilde{\mathscr{N}}_{h,\tau}(\boldsymbol{\theta})\begin{bmatrix}c_{\boldsymbol{\theta},1}^{k-1}\\c_{\boldsymbol{\theta},2}^{k-1}\\\vdots\\c_{\boldsymbol{\theta},M}^{k-1}\end{bmatrix},$$

where

$$\widetilde{\mathscr{M}}_{h,\tau}(\boldsymbol{\theta})=\begin{bmatrix}\frac{1}{\tau}\widehat{M}_{B_h}(\boldsymbol{\theta})+\frac{1}{2}\widehat{M}_{A_h}(\boldsymbol{\theta}) & 0 & \cdots & 0\\-\frac{1}{\tau}\widehat{M}_{B_h}(\boldsymbol{\theta})+\frac{1}{2}\widehat{M}_{A_h}(\boldsymbol{\theta}) & \frac{1}{\tau}\widehat{M}_{B_h}(\boldsymbol{\theta})+\frac{1}{2}\widehat{M}_{A_h}(\boldsymbol{\theta}) & \cdots & 0\\\vdots & \ddots & \ddots & \vdots\\ & \cdots & -\frac{1}{\tau}\widehat{M}_{B_h}(\boldsymbol{\theta})+\frac{1}{2}\widehat{M}_{A_h}(\boldsymbol{\theta}) & \frac{1}{\tau}\widehat{M}_{B_h}(\boldsymbol{\theta})+\frac{1}{2}\widehat{M}_{A_h}(\boldsymbol{\theta})\end{bmatrix}.$$

We can obtain $\widetilde{\mathscr{N}}_{h,\tau}(\boldsymbol{\theta})$ as $\widetilde{\mathscr{M}}_{h,\tau}(\boldsymbol{\theta})$ by only substituting $\widehat{M}_{B_h}(\boldsymbol{\theta}),\widehat{M}_{A_h}(\boldsymbol{\theta})$ with $\widehat{N}_{B_h}(\boldsymbol{\theta}),\widehat{N}_{A_h}(\boldsymbol{\theta})$ in the above matrices We can immediately define the smoothing factor of the Gauss-Seidel relaxation operator by considering its symbol $\widetilde{\mathscr{S}}_{h,\tau}(\boldsymbol{\theta})=\widetilde{\mathscr{M}}_{h,\tau}^{-1}(\boldsymbol{\theta})\widetilde{\mathscr{N}}_{h,\tau}(\boldsymbol{\theta})$, that is

$$\mu=\sup_{\Theta_h\setminus\Theta_{2h}}\left(\rho\left(\widetilde{\mathscr{S}}_{h,\tau}(\boldsymbol{\theta})\right)\right). \tag{10}$$

2.4 Coarse-grid correction analysis

Now, we present the analysis of the coarse-grid correction method. As before, we investigate the effect of the coarse-grid correction, C_h^{2h}, on Fourier modes. The coarse-grid correction operator is given by:

$$C_h^{2h}=I_h-I_{2h}^h(B_{2h}D_t+\Sigma_t A_{2h})^{-1}I_h^{2h}(B_hD_t+\Sigma_t A_h), \tag{11}$$

where D_t and Σ_t are operators corresponding to the Crank-Nicolson approach and I_h, I_{2h}^h, I_h^{2h} are the identity operators, and the transfer operators from coarse to fine grids and vice versa. Also, $(B_{2h}D_t + \Sigma A_{2h})$ and $(B_hD_t + \Sigma A_h)$ are the coarse- and fine-grid operators, respectively.

Our analysis has to take into account the fact that some of the Fourier modes $\varphi(\boldsymbol{\theta},\cdot)$ on the fine grid coincide on $\mathscr{Q}_{2h}$. For any low frequency $\boldsymbol{\theta}^{00} = (\theta_1,\theta_2) \in \Theta_{2h}$, we consider the frequencies $\boldsymbol{\theta}^{\alpha} = \boldsymbol{\theta}^{00} - (\alpha_1 \text{sign}(\theta_1), \alpha_2 \text{sign}(\theta_2))\frac{\pi}{h}$, where, $\alpha = \{(\alpha_1,\alpha_2)|\alpha_j \in \{0,1\}, j = 1,2\}$. The corresponding four Fourier modes $\varphi_h(\boldsymbol{\theta}^{\alpha},\cdot)$ are called harmonics of each other and they form the space of $2h-$ harmonics for $\boldsymbol{\theta}^{00} \in \Theta_{2h}$, as follows

$$\mathscr{F}_{2h}(\boldsymbol{\theta}) = \text{span}\{\varphi(\boldsymbol{\theta}^{00},\cdot), \varphi(\boldsymbol{\theta}^{11},\cdot), \varphi(\boldsymbol{\theta}^{10},\cdot), \varphi(\boldsymbol{\theta}^{01},\cdot)\}.$$

The space of $2h-$harmonics is invariant under the coarse-grid correction operator. Then, the representation of C_h^{2h} on space $\mathscr{F}_{2h}$ is a 4×4 matrix $\widehat{C}_h^{2h}(\boldsymbol{\theta})$. To be more precise, we define two vectors: $\varphi(\boldsymbol{\theta},\cdot) = (\varphi(\boldsymbol{\theta}^{00},\cdot), \varphi(\boldsymbol{\theta}^{11},\cdot), \varphi(\boldsymbol{\theta}^{10},\cdot),\ \varphi(\boldsymbol{\theta}^{01},\cdot))$ and $\mathbf{c}_{\boldsymbol{\theta}}^k(t) = (c_{\boldsymbol{\theta}^{00}}^k(t), c_{\boldsymbol{\theta}^{11}}^k(t),\ c_{\boldsymbol{\theta}^{10}}^k(t),\ c_{\boldsymbol{\theta}^{01}}^k(t))$, and then, the error at the k-th iteration will be $e_h^k(\mathbf{x},t) = \sum_{\boldsymbol{\theta}\in\Theta_{2h}} \mathbf{c}_{\boldsymbol{\theta}}^k(t)\varphi(\boldsymbol{\theta},\mathbf{x})^T$. After applying the coarse-grid correction operator on this error, we obtain $\sum_{\boldsymbol{\theta}\in\Theta_{2h}} \widehat{C}_h^{2h}(\boldsymbol{\theta})\mathbf{c}_{\boldsymbol{\theta}}^k(t)\cdot\varphi(\boldsymbol{\theta},\cdot)$, where $\widehat{C}_h^{2h}(bt)$ is the following 4×4 matrix

$$\widehat{C}_h^{2h}(\boldsymbol{\theta}) = I_4 - \widehat{I}_{2h}^h(\boldsymbol{\theta})(\widehat{B}_{2h}(\boldsymbol{\theta})D_t + \Sigma\widehat{A}_{2h}(\boldsymbol{\theta}))^{-1}\widehat{I}_h^{2h}(\widehat{B}_h(\boldsymbol{\theta})D_t + \Sigma\widehat{A}_h(\boldsymbol{\theta})),$$

where, I_4 is the 4×4 identity matrix, $\widehat{A}_{2h}(\boldsymbol{\theta})$ and $\widehat{B}_{2h}(\boldsymbol{\theta})$ are 1×1 symbols of the discrete operators on the coarse grid, and the rest of involved Fourier symbols are given by:

$$\begin{aligned}
\widehat{A}_h(\boldsymbol{\theta}) &= diag\left(\widehat{A}_h(\boldsymbol{\theta}^{00}), \widehat{A}_h(\boldsymbol{\theta}^{11}), \widehat{A}_h(\boldsymbol{\theta}^{10}), \widehat{A}_h(\boldsymbol{\theta}^{01})\right),\\
\widehat{B}_h(\boldsymbol{\theta}) &= diag\left(\widehat{B}_h(\boldsymbol{\theta}^{00}), \widehat{B}_h(\boldsymbol{\theta}^{11}), \widehat{B}_h(\boldsymbol{\theta}^{10}), \widehat{B}_h(\boldsymbol{\theta}^{01})\right),\\
\widehat{I}_{2h}^h(\boldsymbol{\theta}) &= \left(\widehat{I}_{2h}^h(\boldsymbol{\theta}^{00}), \widehat{I}_{2h}^h(\boldsymbol{\theta}^{11}), \widehat{I}_{2h}^h(\boldsymbol{\theta}^{10}), \widehat{I}_{2h}^h(\boldsymbol{\theta}^{01})\right)^T,\\
\widehat{I}_h^{2h}(\boldsymbol{\theta}) &= \left(\widehat{I}_h^{2h}(\boldsymbol{\theta}^{00}), \widehat{I}_h^{2h}(\boldsymbol{\theta}^{11}), \widehat{I}_h^{2h}(\boldsymbol{\theta}^{10}), \widehat{I}_h^{2h}(\boldsymbol{\theta}^{01})\right).
\end{aligned}$$

Now, by considering the time discretization of operators D_t and Σ_t, we obtain the following $M\times M$ matrices:

$$D_t = \frac{1}{\tau}\begin{bmatrix} 1 & 0 & \cdots & 0\\ -1 & 1 & \cdots & 0\\ \vdots & \ddots & \ddots & \vdots\\ 0 & \cdots & -1 & 1\end{bmatrix}, \quad \Sigma_t = \frac{1}{2}\begin{bmatrix} 1 & 0 & \cdots & 0\\ 1 & 1 & \cdots & 0\\ \vdots & \ddots & \ddots & \vdots\\ 0 & \cdots & 1 & 1\end{bmatrix}.$$

Then, by substituting them the error after application of the coarse grid correction is given by $\widetilde{\mathscr{C}}_{h,\tau}^{2h}(\boldsymbol{\theta})\mathbf{c}_{\boldsymbol{\theta}}^k(t)\cdot\varphi(\boldsymbol{\theta},\cdot)^T$, where the $4M\times 4M$ matrix $\widetilde{\mathscr{C}}_{h,\tau}^{2h}(\boldsymbol{\theta})$ is:

$$\widetilde{\mathscr{C}}_{h,\tau}^{2h}(\boldsymbol{\theta}) = I_{4M} - \widetilde{\mathscr{I}}_{2h}^h(\boldsymbol{\theta})\left(\widetilde{\mathscr{K}}_{2h,\tau}(\boldsymbol{\theta})\right)^{-1}\widetilde{\mathscr{I}}_h^{2h}(\boldsymbol{\theta})\widetilde{\mathscr{K}}_{h,\tau}(\boldsymbol{\theta}),$$

such that I_{4M} is the identity matrix of order $4M$ and $\widetilde{\mathscr{K}_{h,\tau}}(\boldsymbol{\theta})$ is a $4M \times 4M$ matrix defined as:

$$\widetilde{\mathscr{K}_{h,\tau}}(\boldsymbol{\theta}) = \begin{bmatrix} \widetilde{\mathscr{K}_{h,\tau}}(\boldsymbol{\theta}^{00}) & 0 & 0 & 0 \\ 0 & \widetilde{\mathscr{K}_{h,\tau}}(\boldsymbol{\theta}^{11}) & 0 & 0 \\ 0 & 0 & \widetilde{\mathscr{K}_{h,\tau}}(\boldsymbol{\theta}^{10}) & 0 \\ 0 & 0 & 0 & \widetilde{\mathscr{K}_{h,\tau}}(\boldsymbol{\theta}^{01}) \end{bmatrix},$$

with the following blocks in the diagonal:

$$\widetilde{\mathscr{K}_{h,\tau}}(\boldsymbol{\theta}^{\alpha}) = \frac{1}{2\tau} \begin{bmatrix} 2\widehat{B}_h(\boldsymbol{\theta}^{\alpha}) + \tau\widehat{A}_h(\boldsymbol{\theta}^{\alpha}) & & \cdots & 0 \\ -2\widehat{B}_h(\boldsymbol{\theta}^{\alpha}) + \tau\widehat{A}_h(\boldsymbol{\theta}^{\alpha}) & 2\widehat{B}_h(\boldsymbol{\theta}^{\alpha}) + \tau\widehat{A}_h(\boldsymbol{\theta}^{\alpha}) & \cdots & 0 \\ \vdots & \ddots & \ddots & \vdots \\ 0 & \cdots & -2\widehat{B}_h(\boldsymbol{\theta}^{\alpha}) + \tau\widehat{A}_h(\boldsymbol{\theta}^{\alpha}) & 2\widehat{B}_h(\boldsymbol{\theta}^{\alpha}) + \tau\widehat{A}_h(\boldsymbol{\theta}^{\alpha}) \end{bmatrix},$$

where $\alpha = \{(\alpha_1, \alpha_2) | \alpha_j \in \{0,1\}, j = 1,2\}$. In a similar way, we can obtain the Fourier representation of the prolongation and restriction operators, that are $4M \times M$ and $M \times 4M$ matrices, respectively,

$$\widetilde{\mathscr{I}_{2h}^{h}}(\boldsymbol{\theta}) = \left(\widehat{I}_{2h}^{h}(\boldsymbol{\theta}^{00})I_M, \widehat{I}_{2h}^{h}(\boldsymbol{\theta}^{11})I_M, \widehat{I}_{2h}^{h}(\boldsymbol{\theta}^{10})I_M, \widehat{I}_{2h}^{h}(\boldsymbol{\theta}^{01})I_M\right)^T,$$

$$\widetilde{\mathscr{I}_{h}^{2h}}(\boldsymbol{\theta}) = \left(\widehat{I}_{h}^{2h}(\boldsymbol{\theta}^{00})I_M, \widehat{I}_{h}^{2h}(\boldsymbol{\theta}^{11})I_M, \widehat{I}_{h}^{2h}(\boldsymbol{\theta}^{10})I_M, \widehat{I}_{h}^{2h}(\boldsymbol{\theta}^{01})I_M\right).$$

2.5 Two-grid analysis

Now, we are ready to perform the semi-algebraic two-grid analysis. We do this by combining the presented Fourier smoothing analysis and the Fourier analysis for the coarse-grid correction operator. The two-grid operator is defined as $\mathscr{T}_{h,\tau}^{2h} = \mathscr{S}_{h,\tau}^{\nu_2}\mathscr{C}_{h,\tau}^{2h}\mathscr{S}_{h,\tau}^{\nu_1}$, where, $\mathscr{S}_{h,\tau}$ is the smoothing operator such that the number of pre- and post-smoothing iterations are defined by ν_1 and ν_2, respectively and $\mathscr{C}_{h,\tau}^{2h}$ is the coarse-grid correction operator.

The invariant property of the two-grid method comes from the invariant property of both components of this method. To be more precise, the coarse-grid correction operator, $\mathscr{C}_{h,\tau}^{2h}$, and the considered Gauss-Seidel smoothing operator, $\mathscr{S}_{h,\tau}$, both leave the space of $2h-$harmonics $\mathscr{F}_{2h}(\boldsymbol{\theta}^{00})$ invariant for an arbitrary Fourier frequency $\boldsymbol{\theta}^{00} \in \Theta_{2h}$.

Let us assume again that the error at the kth iteration is unique as $\mathbf{c}_{\boldsymbol{\theta}}^{k}(t) \cdot \boldsymbol{\varphi}(\boldsymbol{\theta}, \cdot)^T$. By using the discretization of operators D_t and Σ_t we can obtain the relation $\widetilde{\mathscr{T}_{h,\tau}^{2h}}(\boldsymbol{\theta})\mathbf{c}_{\boldsymbol{\theta}}^{k}(t) \cdot \boldsymbol{\varphi}(\boldsymbol{\theta}, \cdot)^T$ that is the error after the application of the two-grid method, with $\widetilde{\mathscr{T}_{h,\tau}^{2h}}(\boldsymbol{\theta})$ a $4M \times 4M$ matrix, given by

$$\widetilde{\mathscr{T}_{h,\tau}^{2h}}(\boldsymbol{\theta}) = \widetilde{\mathscr{S}_{h,\tau}^{\nu_2}}(\boldsymbol{\theta}) \left(I_{4M} - \widetilde{\mathscr{I}_{2h}^{h}}(\boldsymbol{\theta}) \left(\widetilde{\mathscr{K}_{2h,\tau}}(\boldsymbol{\theta})\right)^{-1} \widetilde{\mathscr{I}_{h}^{2h}}(\boldsymbol{\theta})\widetilde{\mathscr{K}_{h,\tau}}(\boldsymbol{\theta})\right) \widetilde{\mathscr{S}_{h,\tau}^{\nu_1}}(\boldsymbol{\theta}).$$

By considering the Gauss-Seidel smoothing operator, the structure of matrix $\widetilde{\mathscr{S}_{h,\tau}}(\boldsymbol{\theta})$ is as follows

$$\widetilde{\mathscr{S}_{h,\tau}}(\boldsymbol{\theta}) = \begin{bmatrix} \widetilde{\mathscr{S}_{h,\tau}}(\boldsymbol{\theta}^{00}) & 0 & 0 & 0 \\ 0 & \widetilde{\mathscr{S}_{h,\tau}}(\boldsymbol{\theta}^{11}) & 0 & 0 \\ 0 & 0 & \widetilde{\mathscr{S}_{h,\tau}}(\boldsymbol{\theta}^{10}) & 0 \\ 0 & 0 & 0 & \widetilde{\mathscr{S}_{h,\tau}}(\boldsymbol{\theta}^{01}) \end{bmatrix},$$

where the matrix $\widetilde{\mathscr{S}_{h,\tau}}(\boldsymbol{\theta}^{\alpha})$, for $\alpha = \{(\alpha_1,\alpha_2)|\alpha_j \in \{0,1\}, j = 1,2\}$ has been previously described in detail. Finally, we can define the estimation of the two-grid convergence factor by the following

$$\rho = \sup_{\boldsymbol{\theta}\in\Theta_{2h}} \left(\rho\left(\widetilde{\mathscr{T}}^{2h}_{h,\tau}(\boldsymbol{\theta})\right)\right). \tag{12}$$

2.6 Results in two dimensions

In this section, we consider two numerical examples to compare the two-grid convergence factor predicted by SAMA with the asymptotic convergence factor of W-cycle experimentally computed.

When dealing with finite element discretizations of PDEs, the large sparse stiffness and mass matrices are typically built by the standard assembly procedure, [6]. In the case of dealing with a structured grid, however, it suffices to represent the discrete operators by means of stencils, see [1]. We distinguish the stencil form of the rectangular and triangular mesh in presenting stiffness and mass matrices since triangular mesh has the property that their representation in stencil form is different due to the changes in the basis $\{\mathbf{e}'_1,\mathbf{e}'_2\}$. In both cases, we will start with obtaining stencil forms of matrices B_h, A_h, and transfer operators. We will then present the numerical results that are performed by Matlab.

2.6.1 Case 1: rectangular mesh

The first numerical experiment deals with the solution of the two-dimensional heat equation (1) considering $\Omega = [0,2]^2$ where Dirichlet boundary and initial conditions are chosen in such a way that the analytic solution equals

$$u(x_1,x_2,t) = t^2 \sin(\frac{\pi x_1}{2}) \sin(\frac{\pi x_2}{2}).$$

We consider the bilinear basis function, $a+bx+cy_dxy$, to obtain stiffness and mass matrices $A_h = \{a(\phi_i,\phi_j)\}$, $B_h = \{(\phi_i,\phi_j)\}$, introduced in introduction part. It leads to the following ODE system,

$$B_h\dot{\mathbf{u}}_h(t) + A_h\mathbf{u}_h(t) = F_h(t), \quad \mathbf{u}_h(0) = g_h, \quad t > 0.$$

Which the stencil forms of A_h, and B_h are as follows:

$$B_h = \frac{h^2}{36}\begin{bmatrix} 1 & 4 & 1 \\ 4 & 16 & 4 \\ 1 & 4 & 1 \end{bmatrix}, \qquad A_h = \frac{1}{3}\begin{bmatrix} -1 & -1 & -1 \\ -1 & 8 & -1 \\ -1 & -1 & -1 \end{bmatrix}.$$

We pick the waveform relaxation (WR) method to solve this equation. The WR method is based on splitting matrices A_h, B_h as $A_h = M_{h_A} - N_{h_A}$, $B_h = M_{h_B} - N_{h_B}$, leading to the following iteration:

$$M_{B_h}\dot{\mathbf{u}}^k_h(t) + M_{A_h}\mathbf{u}^k_h(t) = N_{B_h}\dot{\mathbf{u}}^{k-1}_h(t) + N_{A_h}\mathbf{u}^{k-1}_h(t) + F_h(t). \tag{13}$$

If we consider decomposition of matrices A_h and B_h as $A_h = -L_{A_h} + D_{A_h} - U_{A_h}$ and $B_h = -L_{B_h} + D_{B_h} - U_{B_h}$, we can define the Gauss-Seidel waveform relaxation as bellow:

$$\begin{aligned} M_{A_h} &= -L_{A_h} + D_{A_h}, \quad N_{A_h} = U_{A_h}, \\ M_{B_h} &= -L_{B_h} + D_{B_h}, \quad N_{B_h} = U_{B_h}. \end{aligned}$$

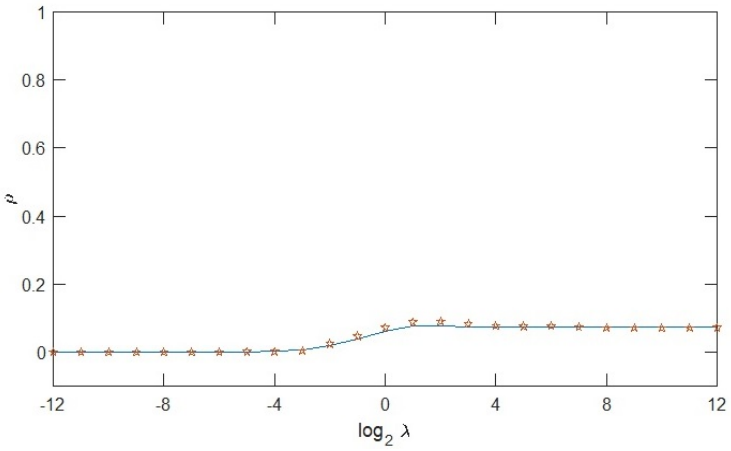

Figure 3: Two-grid convergence factor predicted by analysis and experimentally convergence factor computed by W(1,1)-cycle for various parameter $\lambda = \tau/h^2$ and with bilinear basis functions.

where also $\mathbf{u}_h^k(0) = g_h$, for $k \geq 1$ and $\mathbf{u}_h^k(t)$ indicates the approximation of $\mathbf{u}(t)$ at iteration k. It is natural to define $\mathbf{u}_h^0(t)$ along the whole time interval equal to the initial condition, i.e $\mathbf{u}_h^0(t) = g_h$, $t > 0$.

As you can see it is a semi-discretization only in space. Now, using the Crank-Nicolson approach for the time discretization we obtain a space-time multigrid method with coarsening only in space. Indeed, we have time-line Gauss-Seidel waveform relaxation, with standard full weighting restriction and linear interpolation in space for data transfer between the levels in the multigrid hierarchy.

To apply the presented analysis we also need to define the components of the multigrid waveform relaxation method. As we stated in the previous sections a Gauss-Seidel waveform relaxation is considered. Regarding the intergrid transfer operators, the stencil of the restriction operator, I_h^{2h}, is given by

$$I_h^{2h} = \frac{1}{16}\begin{bmatrix} 1 & 2 & 1 \\ 2 & 4 & 2 \\ 1 & 2 & 1 \end{bmatrix},$$

The prolongation operator I_{2h}^h, is obtained according to the relation $I_h^{2h} = \frac{1}{4} I_{2h}^h$, see Algorithm 1 and [12], [14] for more details.

In Figure 3, we show the comparative results, where the two-grid convergence factors predicted by SAMA are illustrated together with the asymptotic convergence rates obtained by using a W-cycle multigrid waveform relaxation depending on the parameter $\lambda = \tau/h^2$, which represents the anisotropy in the operator ranging from 2^{-12} to 2^{12}. In this Figure, two smoothing steps are considered and the number of time steps is set to 32 ($M = 32$). Moreover, the multigrid waveform relaxation results are calculated by considering a random initial guess and a zero right-hand side. As we can see, the analysis results of SAMA and the rates experimentally computed match very accurately.

Also in the first row of Table 1, the asymptotic convergence factor computed by W(1,1)-cycle together with their predicted results by SAMA (in parentheses) are displayed for different values of τ and a fixed grid size $64 \times 64 \times 32$. Through these considerations, we can also observe an accurate match between the experimental and the predicted results. In the second row of Table 1 we substitute the matrix

Table 1: Two-grid convergence factor predicted by SAMA and the asymptotic convergence factor (between paranteces) for several values of τ when $M = 32$ and $h = 2^{-5}$ in two dimensions with linear and bilinear basis functions. The matrices B_h =mass and B_h =Identity are corresponding to the finite element and finite differences methods, respectively.

	B \ τ	0.04	0.02	0.01	0.005	0.0025	0.001
bilinear basis	Mass	0.0710 (0.0704)	0.0702 (0.0730)	0.0681 (0.0761)	0.0646 (0.0776)	0.0576 (0.0729)	0.0425 (0.0583)
	Identity	0.0724 (0.0711)	0.0728 (0.0732)	0.0743 (0.0765)	0.0776 (0.0782)	0.0779 (0.0721)	0.0624 0.0549
linear basis	Mass	0.2697 (0.2439)	0.2670 (0.2506)	0.2616 (0.2548)	0.2510 (0.2596)	0.2283 (0.2445)	0.1752 (0.1853)
	Identity	0.2704 (0.2368)	0.2682 (0.2412)	0.2637 (0.2483)	0.2549 (0.2503)	0.2348 (0.2391)	0.1818 (0.1863)

B_h by the identity matrix. One can see that the results when choosing B_h as the identity matrix match with the case in which the applied discretization method is the finite difference scheme [5].

2.6.2 Case 2: triangular mesh

In this case, we consider the two-dimensional heat equation (1) on a parallelogram domain that is constructed from two identical triangles. To specify the triangle, we consider the geometric parameters using two angles of a triangle, denoted by α and β. Such that, these angles satisfy the relation $\beta = \pi - \gamma$ and $\alpha < \gamma$, see Figure 4. Dirichlet boundary and initial conditions are chosen such that the analytic solution is

$$u(x_1,x_2,t) = t^2 x_2(x_2 - x_1\tan\alpha)(x_2 - x_1\tan\alpha + \tan\alpha)\left(x_2 - \frac{1}{\cot\alpha + \cot\beta}\right).$$

Applying a linear finite element discretization on a regular triangular mesh, in such a way that each triangle of Figure 4 is divided into four congruent triangles connecting the midpoints of their edges and this is repeated until a regular triangular mesh is obtained, we can easily find

$$B_h\dot{\mathbf{u}}_h(t) + A_h\mathbf{u}_h(t) = F_h(t), \quad \mathbf{u}_h(0) = g_h, \quad t > 0.$$

As presented in the previous case we need to define the mass and stiffness stencils. First, we explain briefly the stiffness stencil, presented in [11], then we construct the mass stencil.

Let H be a hexagon composed of six congruent triangles T_i such that it is the support of the basis function $\phi_{n,m}$ associated with the node $\mathbf{x}_{n,m}$ where $\mathbf{x}_{n,m}$ is the center node of the hexagon H and also an interior node of a triangle of the coarsest grid. The vertices of this hexagon are $\mathbf{x}_{n+1,m}$, $\mathbf{x}_{n-1,m}$, $\mathbf{x}_{n,m+1}$, $\mathbf{x}_{n,m-1}$, $\mathbf{x}_{n+1,m+1}$, $\mathbf{x}_{n-1,m-1}$, see Figure 5 (right).

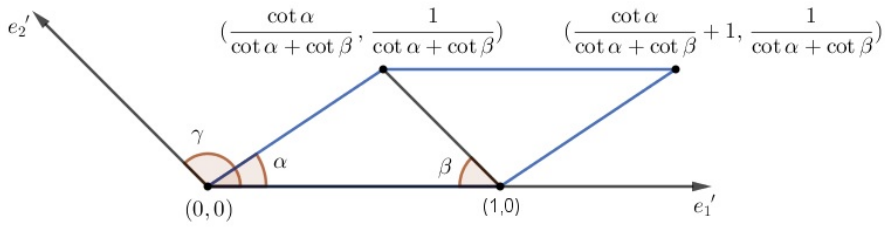

Figure 4: Considered domain for example 2 by the coarsest grid.

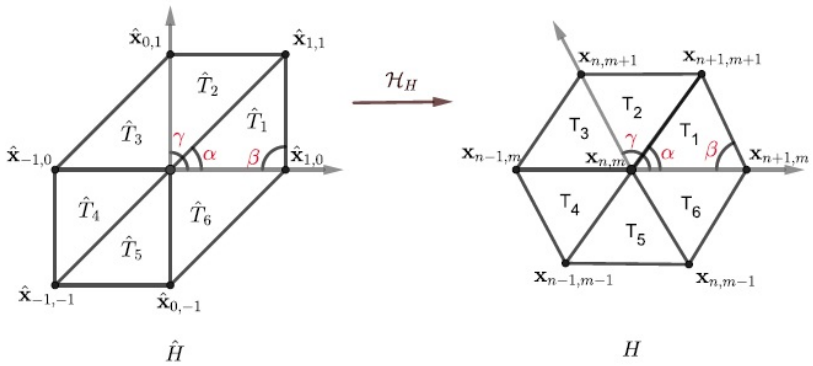

Figure 5: Hexagon around an interior point of a general triangle, with angles α and β, together with its affine mapping $\mathscr{H}_H$ and corresponding coordinates.

The stiffness stencil associated to node $\mathbf{x}_{n,m}$ is

$$A = \begin{bmatrix} 0 & \int_{T_2\cup T_3} \nabla\phi_{n,m+1}\cdot\nabla\phi_{n,m}\,\mathrm{d}\mathbf{x} & \int_{T_1\cup T_2} \nabla\phi_{n+1,m+1}\cdot\nabla\phi_{n,m}\,\mathrm{d}\mathbf{x} \\ \int_{T_3\cup T_4} \nabla\phi_{n-1,m}\cdot\nabla\phi_{n,m}\,\mathrm{d}\mathbf{x} & \int_{\cup_{i=1}^{6}} \nabla\phi_{n,m}\cdot\nabla\phi_{n,m}\,\mathrm{d}\mathbf{x} & \int_{T_1\cup T_6} \nabla\phi_{n+1,m}\cdot\nabla\phi_{n,m}\,\mathrm{d}\mathbf{x} \\ \int_{T_4\cup T_5} \nabla\phi_{n-1,m-1}\cdot\nabla\phi_{n,m}\,\mathrm{d}\mathbf{x} & \int_{T_5\cup T_6} \nabla\phi_{n,m-1}\cdot\nabla\phi_{n,m}\,\mathrm{d}\mathbf{x} & 0 \end{bmatrix}.$$

We use hexagon $\hat{H}$ with center $\mathbf{x}_{0,0}$ and vertices $\hat{\mathbf{x}}_{1,0}, \hat{\mathbf{x}}_{-1,0}, \hat{\mathbf{x}}_{0,1}, \hat{\mathbf{x}}_{0,-1}, \hat{\mathbf{x}}_{1,1}, \hat{\mathbf{x}}_{-1,-1}$ as the reference grid for computational purpose, see Figure 5 (left). Mapping hexagon $\hat{H}$ to H is given by an affine transformation $\mathscr{H}_H$ such that $\mathbf{x} = \mathscr{H}_H(\hat{\mathbf{x}}) = \mathscr{D}_H\hat{\mathbf{x}} + d_H$, yielding $\mathscr{H}_H(\hat{\mathbf{x}}_{k,l}) = \mathbf{x}_{n+k,m+l}$. This affine transformation can be simply defined as follows:

$$\mathscr{D}_H = \begin{bmatrix} x_{n+1,m} - x_{n,m} & x_{n+1,m+1} - x_{n+1,m} \\ y_{n+1,m} - y_{n,m} & y_{n+1,m+1} - y_{n+1,m} \end{bmatrix}, \qquad d_H = \begin{bmatrix} x_{n,m} \\ y_{n,m} \end{bmatrix}.$$

where $(x_{k,l}, y_{k,l})$ are the coordinates of the node $\mathbf{x}_{k,l}$. Using defined transformation the degrees of freedom and basis functions on the reference hexagon $\hat{H}$, $\hat{\phi}$, can be transformed to the degrees of freedom and basis functions on the arbitrary hexagon H, ϕ, given by $\hat{\phi}_{k,l} = \phi_{n+k,m+l} \circ \mathscr{H}$. By these consideration

after applying the change of variable associated with the affine map $\mathscr{H}$, the stiffness stencil satisfys the following expression

$$A_h = |\det \mathscr{D}_H| \begin{bmatrix} 0 & a_{0,1} & a_{1,1} \\ a_{-1,0} & a_{0,0} & a_{1,0} \\ a_{-1,-1} & a_{0,-1} & 0 \end{bmatrix},$$

where

$$\begin{aligned}
a_{0,1} &= \int_{\hat{T}_2} (\mathscr{D}_H^{-1})^t \nabla\hat{\phi}_{0,1} \cdot (\mathscr{D}_H^{-1})^t \nabla\hat{\phi}_{0,0} d\hat{\mathbf{x}} + \int_{\hat{T}_3} (\mathscr{D}_H^{-1})^t \nabla\hat{\phi}_{0,1} \cdot (\mathscr{D}_H^{-1})^t \nabla\hat{\phi}_{0,0} d\hat{\mathbf{x}}, \\
a_{1,1} &= \int_{\hat{T}_1} (\mathscr{D}_H^{-1})^t \nabla\hat{\phi}_{1,1} \cdot (\mathscr{D}_H^{-1})^t \nabla\hat{\phi}_{0,0} d\hat{\mathbf{x}} + \int_{\hat{T}_2} (\mathscr{D}_H^{-1})^t \nabla\hat{\phi}_{1,1} \cdot (\mathscr{D}_H^{-1})^t \nabla\hat{\phi}_{0,0} d\hat{\mathbf{x}}, \\
a_{-1,0} &= \int_{\hat{T}_3} (\mathscr{D}_H^{-1})^t \nabla\hat{\phi}_{-1,0} \cdot (\mathscr{D}_H^{-1})^t \nabla\hat{\phi}_{0,0} d\hat{\mathbf{x}} + \int_{\hat{T}_4} (\mathscr{D}_H^{-1})^t \nabla\hat{\phi}_{-1,0} \cdot (\mathscr{D}_H^{-1})^t \nabla\hat{\phi}_{0,0} d\hat{\mathbf{x}}, \\
a_{0,0} &= \sum_{i=1}^{6} \int_{\hat{T}_i} (\mathscr{D}_H^{-1})^t \nabla\hat{\phi}_{0,0} \cdot (\mathscr{D}_H^{-1})^t \nabla\hat{\phi}_{0,0} d\hat{\mathbf{x}}, \\
a_{1,0} &= \int_{\hat{T}_1} (\mathscr{D}_H^{-1})^t \nabla\hat{\phi}_{1,0} \cdot (\mathscr{D}_H^{-1})^t \nabla\hat{\phi}_{0,0} d\hat{\mathbf{x}} + \int_{\hat{T}_6} (\mathscr{D}_H^{-1})^t \nabla\hat{\phi}_{1,0} \cdot (\mathscr{D}_H^{-1})^t \nabla\hat{\phi}_{0,0} d\hat{\mathbf{x}}, \\
a_{-1,-1} &= \int_{\hat{T}_4} (\mathscr{D}_H^{-1})^t \nabla\hat{\phi}_{-1,-1} \cdot (\mathscr{D}_H^{-1})^t \nabla\hat{\phi}_{0,0} d\hat{\mathbf{x}} + \int_{\hat{T}_5} (\mathscr{D}_H^{-1})^t \nabla\hat{\phi}_{-1,-1} \cdot (\mathscr{D}_H^{-1})^t \nabla\hat{\phi}_{0,0} d\hat{\mathbf{x}}, \\
a_{0,-1} &= \int_{\hat{T}_5} (\mathscr{D}_H^{-1})^t \nabla\hat{\phi}_{0,-1} \cdot (\mathscr{D}_H^{-1})^t \nabla\hat{\phi}_{0,0} d\hat{\mathbf{x}} + \int_{\hat{T}_6} (\mathscr{D}_H^{-1})^t \nabla\hat{\phi}_{0,-1} \cdot (\mathscr{D}_H^{-1})^t \nabla\hat{\phi}_{0,0} d\hat{\mathbf{x}}.
\end{aligned}$$

Considering

$$C_H = \mathscr{D}_H^{-1} (\mathscr{D}_H^{-1})^t = \begin{bmatrix} c_{11}^H & c_{12}^H \\ c_{21}^H & c_{22}^H \end{bmatrix},$$

we can obtain $A_h = |\det \mathscr{D}_H| \left(c_{11}^H \hat{A}_{xx} + (c_{12}^H + c_{21}^H) \hat{A}_{xy} + c_{22}^H \hat{A}_{yy} \right)$, where

$$\hat{A}_{xx} = \begin{bmatrix} 0 & 0 & 0 \\ -1 & 2 & -1 \\ 0 & 0 & 0 \end{bmatrix}, \quad \hat{A}_{xy} = \begin{bmatrix} 0 & 1 & -1 \\ -1 & 2 & -1 \\ -1 & 1 & 0 \end{bmatrix}, \quad \hat{A}_{xx} = \begin{bmatrix} 0 & -1 & 0 \\ 0 & 2 & 0 \\ 0 & -1 & 0 \end{bmatrix},$$

are the stencils respectively related to the operators $-\partial_{xx}$, $-\partial_{xy}$ and $-\partial_{yy}$ in the reference hexagon. In the special limit case $\beta = \pi/2$ (or in the opposite direction $\alpha = \pi/2$, [4]), the stiffness stencil will be obtained as the same as the classical five points finite difference discretization of the Laplace operator for rectangular grids,

$$A_h = \frac{1}{h^2} \begin{bmatrix} & -1 & \\ -1 & 4 & -1 \\ & -1 & \end{bmatrix}.$$

The coefficients of stencil B_h on hexagon H can be presented by the following equations

$$
\begin{aligned}
s_{0,1} &= \mid \det \mathscr{D}_H \mid \left(\int_{\hat{T}_1} \widehat{\phi}_{0,1} \widehat{\phi}_{0,0} \, \mathrm{d}\widehat{\mathbf{x}} + \int_{\widehat{T}_2} \widehat{\phi}_{0,1} \hat{\phi}_{0,0} \, \mathrm{d}\widehat{\mathbf{x}} \right), \\
s_{-1,0} &= \mid \det \mathscr{D}_H \mid \left(\int_{\hat{T}_3} \widehat{\phi}_{-1,0} \widehat{\phi}_{0,0} \, \mathrm{d}\widehat{\mathbf{x}} + \int_{\widehat{T}_4} \widehat{\phi}_{-1,0} \hat{\phi}_{0,0} \, \mathrm{d}\widehat{\mathbf{x}} \right), \\
s_{1,1} &= \mid \det \mathscr{D}_H \mid \left(\int_{\hat{T}_2} \widehat{\phi}_{1,1} \widehat{\phi}_{0,0} \, \mathrm{d}\widehat{\mathbf{x}} + \int_{\widehat{T}_3} \widehat{\phi}_{1,1} \hat{\phi}_{0,0} \, \mathrm{d}\widehat{\mathbf{x}} \right), \\
s_{1,0} &= \mid \det \mathscr{D}_H \mid \left(\int_{\hat{T}_1} \widehat{\phi}_{1,0} \widehat{\phi}_{0,0} \, \mathrm{d}\widehat{\mathbf{x}} + \int_{\widehat{T}_6} \widehat{\phi}_{1,0} \hat{\phi}_{0,0} \, \mathrm{d}\widehat{\mathbf{x}} \right), \\
s_{0,0} &= \mid \det \mathscr{D}_H \mid \left(\sum_{i=1}^{6} \int_{\hat{T}_i} \widehat{\phi}_{0,0} \widehat{\phi}_{0,0} \, \mathrm{d}\widehat{\mathbf{x}} \right), \\
s_{0,-1} &= \mid \det \mathscr{D}_H \mid \left(\int_{\hat{T}_5} \widehat{\phi}_{0,-1} \widehat{\phi}_{0,0} \, \mathrm{d}\widehat{\mathbf{x}} + \int_{\widehat{T}_6} \widehat{\phi}_{0,-1} \hat{\phi}_{0,0} \, \mathrm{d}\widehat{\mathbf{x}} \right), \\
s_{-1,-1} &= \mid \det \mathscr{D}_H \mid \left(\int_{\hat{T}_4} \widehat{\phi}_{-1,-1} \widehat{\phi}_{0,0} \, \mathrm{d}\widehat{\mathbf{x}} + \int_{\widehat{T}_5} \widehat{\phi}_{-1,-1} \hat{\phi}_{0,0} \, \mathrm{d}\widehat{\mathbf{x}} \right),
\end{aligned}
$$

normalizing the coefficients by $\mid \det \mathscr{D}_H \mid$, we obtain a fixed mass stencil for every triangulation,

$$
B_h = \frac{1}{12} \begin{bmatrix} & 1 & 1 \\ 1 & 6 & 1 \\ 1 & 1 & \end{bmatrix}.
$$

Regarding the intergrid transfer operators, the stencil of the restriction operator, I_h^{2h}, is given by

$$
I_h^{2h} = \frac{1}{8} \begin{bmatrix} & 1 & 1 \\ 1 & 2 & 1 \\ 1 & 1 & \end{bmatrix}.
$$

We can obtain immediately the prolongation operator by the expression $I_h^{2h} = \frac{1}{4} I_{2h}^h$.

In Figure 6, we show the comparative results in the special case $\beta = \pi/2$, where the two-grid convergence factors predicted by SAMA are illustrated together with the asymptotic convergence rates obtained by using a W-cycle multigrid waveform relaxation depending on the parameter $\lambda = \tau/h^2$ ranging from 2^{-12} to 2^{12}. Here, two smoothing steps, a random initial guess, and a zero right-hand side are considered where the number of time steps is set at 32 ($M = 32$). As we can see, the analysis results of SAMA and the rates experimentally computed match very accurately.

Also in the third row of Table 1 , the asymptotic convergence factor computed by W(1,1)-cycle together with their predicted results by SAMA (in parentheses) are displayed for different values of τ and a fixed grid size $64 \times 64 \times 32$. We can observe an accurate match between the experimental and the predicted results. In the 4th row of Table 1 we substitute the matrix B_h by the identity matrix. One can see that the results when choosing B_h as the identity matrix match with the case in which the applied discretization method is the finite difference scheme, [5].

3 Semi-algebraic mode analysis in three dimensions

Now, we describe the convergence analysis of the multigrid waveform relaxation method by SAMA based on the finite element method considering trilinear and nonsymmetric bilinear basis functions respectively on cubic and triangular prism elements. Here, we explain the general components associated with each case. The rest of the analysis can be obtained in a similar way performed in the two-dimensional analysis.

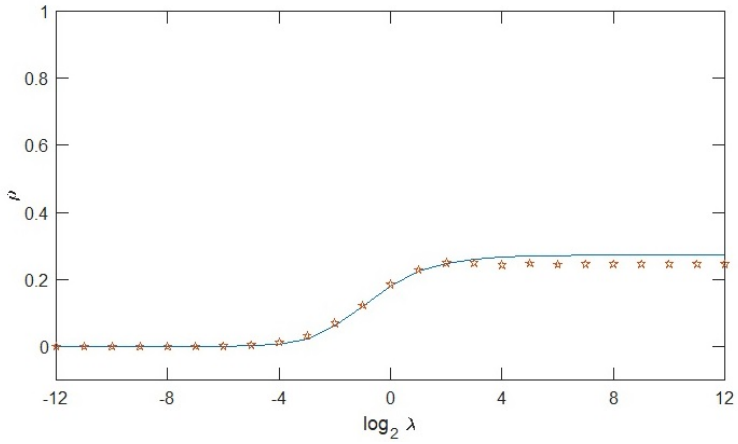

Figure 6: Two-grid convergence factor predicted by analysis and experimentally convergence factor computed by W(1,1)-cycle for various parameter $\lambda = \tau/h^2$ and with linear basis functions where $\beta = 90$.

3.1 General definitions for cubic elements.

We have to perform some changes to the definitions to extend the SAMA from two dimensions to three dimensions. As we did for the two-dimensional case we need to define the infinite grid $\mathscr{Q}_h$,

$$\mathscr{Q}_h = \{\mathbf{x} = \mathbf{kh} = (k_1h_1, k_2h_2, k_3h_3),\ \mathbf{k} \in \mathbb{Z}^3\}.$$

In this case, the Fourier modes are $\varphi(\boldsymbol{\theta}, \mathbf{x}) = e^{i\boldsymbol{\theta}\cdot\mathbf{x}} = e^{i\theta_1 x_1} e^{i\theta_2 x_2} e^{i\theta_3 x_3}$ where $\boldsymbol{\theta} \in \Theta_h = (-\pi/h, \pi/h]^3$. Similar to the two-dimensional case, any discrete grid function for a fixed t can be defined as a formal linear combination of Fourier modes. Also, we obtain a new $8-$dimensional Fourier space generated by one low-frequency Fourier mode $\boldsymbol{\theta} = \boldsymbol{\theta}^{000} \in \Theta_{2h} = (-\pi/2h, \pi/2h]^3$ as follows:

$$\begin{aligned}\mathscr{F}_{2h}(\boldsymbol{\theta}) =& \text{span}\{\varphi(\boldsymbol{\theta}^{000}, \cdot), \varphi(\boldsymbol{\theta}^{111}, \cdot), \varphi(\boldsymbol{\theta}^{100}, \cdot), \varphi(\boldsymbol{\theta}^{011}, \cdot), \varphi(\boldsymbol{\theta}^{010}, \cdot), \varphi(\boldsymbol{\theta}^{101}, \cdot),\\ & \varphi(\boldsymbol{\theta}^{001}, \cdot), \varphi(\boldsymbol{\theta}^{110}, \cdot)\},\end{aligned} \tag{14}$$

such that the high-frequencies are given by the following equation

$$\boldsymbol{\theta}^{\alpha} = \boldsymbol{\theta}^{000} - (\,\alpha_1 \text{sign}(\theta_1), \alpha_2 \text{sign}(\theta_2), \alpha_3 \text{sign}(\theta_3)\,)\,\frac{\pi}{h},$$

where, $\boldsymbol{\theta}^{000} = (\theta_1, \theta_2, \theta_3)$ and $\alpha = \{(\alpha_1, \alpha_2, \alpha_3)\,|\,\alpha_j \in \{0,1\}, j = 1,2,3\}$.

By the above definitions the resulting Fourier representations of the smoothing, coarse-grid correction, and two-grid operators are $8M \times 8M$ matrices that can be computed following the same idea carried out in Sections 2.3 -2.5 for the two-dimensional case. So, in fact, SAMA in three dimensions is based on a three-dimensional spatial LFA combined with an exact analysis of the time variable. The stiffness and mass stencils together with some numerical results for this case are presented in Section 3.3.1.

3.2 General definitions for triangular prism elements.

In this part, we present some preliminary definitions on a triangular prism element. Prism elements deal with some columnar region, in this case, a triangular prism region, that is constructed as the product of

a triangle and an interval. Let $\{e'_1, e'_2, e'_3\}$ be a unitary basis of $\mathbb{R}^3$, $0 < \gamma < \pi$ the angle between e'_1 and e'_2 where e'_3 is orthogonal to both of them. We consider their reciprocal basis as $\{e''_1, e''_2, e''_3\}$ such that $e'_i \cdot e''_j = \delta_{ij}$, $i, j = 1, 2, 3$, where δ_{ij} is Kronecker's delta. Applying variable changes $\mathbf{x} = \mathrm{F}(\mathbf{x}')$, $\boldsymbol{\theta} = \mathrm{G}(\boldsymbol{\theta}'')$ and using the usual Fourier transform and its inversion formula, we can obtain the following expression for inner product in the new bases

$$\mathrm{G}(\boldsymbol{\theta}'') \cdot \mathrm{F}(\mathbf{x}') = \boldsymbol{\theta} \cdot \mathbf{x} = \theta''_1 x'_1 + \theta''_2 x'_2 + \theta''_3 x'_3 = \boldsymbol{\theta}'' \cdot \mathbf{x}'.$$

An infinite grid oriented in the directions e'_1, e'_2 and e'_3 can be defined as follows:

$$\mathscr{G}_h = \{\mathbf{x}' = (x'_1, x'_2, x'_3) | x'_i = k_i h_i, k_i \in \mathbb{Z}, i = 1, 2, 3\},$$

where $\mathbf{h} = (h_1, h_2, h_3)$ such that a typical point in $\mathscr{G}_h$ is given by $x'_1 \mathbf{e}'_1 + x'_2 \mathbf{e}'_2 + x'_3 \mathbf{e}'_3$. Considering the discrete Fourier transform of a grid function, we can define the Fourier modes $\varphi_h(\boldsymbol{\theta}'', \mathbf{x}') = \mathrm{e}^{i\theta''_1 x'_1} \mathrm{e}^{i\theta''_2 x'_2} \mathrm{e}^{i\theta''_3 x'_3}$ and Fourier space $\mathscr{F}(\mathscr{G}_h) = \{\varphi_h(\boldsymbol{\theta}'', \cdot), \boldsymbol{\theta}'' \in \Theta''_h\}$, where $\boldsymbol{\theta}'' = (\theta''_1, \theta''_2, \theta''_3) \in \Theta''_h = (-\pi/h_1, \pi/h_1] \times (-\pi/h_2, \pi/h_2] \times (-\pi/h_3, \pi/h_3]$. Similar to the two-dimensional case, any discrete grid function for a fixed t can be defined as a formal linear combination of Fourier modes. Again here, we obtain a $8-$dimensional Fourier space generated by one low-frequency Fourier mode $\boldsymbol{\theta}'' = \boldsymbol{\theta}''_{000} \in \Theta''_{2h} = (-\pi/2h_1, \pi/2h_1] \times (-\pi/2h_2, \pi/2h_2] \times (-\pi/2h_3, \pi/2h_3]$, it can be defined replacing $\boldsymbol{\theta}$ by $\boldsymbol{\theta}''$ in equation (14).

Due to the fact that in triangular prism mesh the grids and the frequency space are referred to as reciprocal bases, the Fourier modes are in terms of $\boldsymbol{\theta}''$ and $\mathbf{x}'$, the analysis for this case also can be computed following the same idea carried out in Sections 2.3 -2.5.

3.3 Results in three dimensions

In this section, we consider two numerical examples to compare the two-grid convergence factor predicted by SAMA with the asymptotic convergence factor of W-cycle experimentally computed in three dimensions. The first example shows numerical results on the cubic mesh and the second one illustrates the numerical analysis corresponding to the triangular prism elements. Similar to the two-dimensional case, first we define the stencil forms of the mass and stiffness matrices then, we present the comparative results for every case. All numerical computations are performed by MATLAB.

3.3.1 Case 1: Cubic Elements (CE)

Consider the three dimensional heat equation (1) where Dirichlet boundary and initial conditions in such a way that the analytic solution is

$$u(x_1, x_2, t) = t^2 \sin(\frac{\pi x_1}{2}) \sin(\frac{\pi x_2}{2}) \sin(\frac{\pi x_3}{2}).$$

We consider cubic elements to obtaining the following discrete problem,

$$B_h \dot{\mathbf{u}}_h(t) + A\mathbf{u}_h(t) = F_h(t), \quad \mathbf{u}_h(0) = g_h, \quad t > 0.$$

The corresponding stencils computed for the mass and stiffness matrices are respectively as follows:

$$B_h = \frac{1}{216} \left[\begin{bmatrix} 1 & 4 & 1 \\ 4 & 16 & 4 \\ 1 & 4 & 1 \end{bmatrix} \begin{bmatrix} 4 & 16 & 4 \\ 16 & 64 & 16 \\ 4 & 16 & 4 \end{bmatrix} \begin{bmatrix} 1 & 4 & 1 \\ 4 & 16 & 4 \\ 1 & 4 & 1 \end{bmatrix} \right],$$

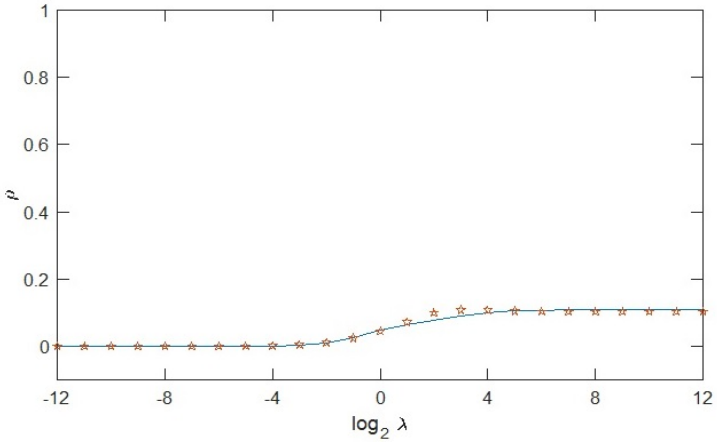

Figure 7: Two-grid convergence factor predicted by analysis and experimentally convergence factor computed by W(1,1)-cycle for various parameter $\lambda = \tau/h^2$ computed on the cubic mesh.

and,

$$A_h = \frac{1}{12h^2}\left[\begin{bmatrix}-1&-2&-1\\-2&0&-2\\-1&-2&-1\end{bmatrix}\begin{bmatrix}-2&0&-2\\0&32&0\\-2&0&-2\end{bmatrix}\begin{bmatrix}-1&-2&-1\\-2&0&-2\\-1&-2&-1\end{bmatrix}\right].$$

To apply the presented analysis we also need to define the components of the multigrid waveform relaxation method. As we stated in the previous sections a Gauss-Seidel waveform relaxation is considered. Regarding the intergrid transfer operators, the stencil of the restriction operator, I_h^{2h}, is given by

$$I_h^{2h} = \frac{1}{64}\left[\begin{bmatrix}1&2&1\\2&4&2\\1&2&1\end{bmatrix}\begin{bmatrix}2&4&2\\4&8&4\\2&4&2\end{bmatrix}\begin{bmatrix}1&2&1\\2&4&2\\1&2&1\end{bmatrix}\right].$$

The prolongation operator I_{2h}^h, is obtained according to the relation $I_h^{2h} = \frac{1}{8}I_{2h}^h$, see [12, 14] for more details.

In Figure 7, we show the comparative results, where the two-grid convergence factors predicted by SAMA are illustrated together with the asymptotic convergence rates obtained by using a W-cycle multigrid waveform relaxation depending on the parameter $\lambda = \tau/h^2$, which represents the anisotropy in the operator ranging from 2^{-12} to 2^{12}. In this Figure, two smoothing steps are considered and the number of time steps is set at 32 ($M = 32$). Moreover, the multigrid waveform relaxation results are calculated by considering a random initial guess and a zero right-hand side. As we can see, the analysis results of SAMA and the rates experimentally computed match very accurate.

Also in the first row of Table 2 , the asymptotic convergence factor computed by W(1,1) cycle together with their predicted results by SAMA (in parentheses) are displayed for different values of τ and a fixed grid size $64 \times 64 \times 32$. We can observe an accurate match between the experimental and the predicted results. In the second row of Table 2 we substitute the matrix B_h by the identity matrix. One can see that the results when choosing B_h as the identity matrix match with the case in which the applied discretization method is the finite difference scheme.

Table 2: Two-grid convergence factor predicted by SAMA and the asymptotic convergence factor (between paranteces) for several values of τ when $M = 32$ and $N = 64$ in three dimensions with triangular prism Elements (PE) and Cubic Elements (CE). The matrices B_h =mass and B_h =Identity are corresponding to the finite element and finite differences methods, respectively.

	B \ τ	0.04	0.02	0.01	0.005	0.0025	0.001
Cubic Elements(CE)	Mass	0.1084 (0.1072)	0.1129 (0.1119)	0.1330 (0.1291)	0.1539 (0.1541)	0.1923 (0.1946)	0.2790 (0.2759)
	Identity	0.0946 (0.0995)	0.0821 (0.0888)	0.0691 (0.0574)	0.0545 (0.0527)	0.0333 (0.0312)	0.0107 (0.0109)
Prism Elements(PE)	Mass	0.1628 (0.1668)	0.1593 (0.1439)	0.1526 (0.1442)	0.1407 (0.1413)	0.1221 (0.1221)	0.0955 (0.1091)
	Identity	0.1664 (0.1671)	0.1505 (0.1635)	0.1268 (0.1378)	0.1004 (0.1049)	0.0676 (0.0710)	0.0303 (0.0308)

3.3.2 Case 2: Triangular Prism Elements (TPE)

In this case, we consider the three dimensional heat equation (1) on a parallelogram prism where the parallelogram shown in Figure 4 is considered. Dirichlet boundary and initial conditions are chosen such that the analytic solution is

$$u(x_1,x_2,x_3,t) = t^2 x_2 x_3 (x_3-1)(x_2 - x_1\tan\alpha)(x_2 - x_1\tan\alpha + \tan\alpha)\left(x_2 - \frac{1}{\cot\alpha + \cot\beta}\right).$$

Considering a uniform triangular prism elements the problem reduces to the following discrete form,

$$B_h \dot{\mathbf{u}}_h(t) + A_h \mathbf{u}_h(t) = F_h(t), \quad \mathbf{u}_h(0) = g_h, \quad t > 0.$$

As presented in the previous cases we need to define the mass and stiffness stencils. To reach to this goal, let $\mathbf{x}_{n,m,k}$ be a central node of a hexagonal prism P, constructed of twelve triangular prism elements, which is the support of a basis function $\phi_{n,m,k}$ associated to it. The eighteen vertices of this hexagonal prism are: $\mathbf{x}_{n+1,m,s}, \mathbf{x}_{n-1,m,s}, \mathbf{x}_{n,m+1,s}, \mathbf{x}_{n,m-1,s}, \mathbf{x}_{n+1,m+1,s}, \mathbf{x}_{n-1,m-1,s}$ where $s = k-1, k, k+1$.

Using a reference hexagonal prism $\hat{P}$ with center $\hat{\mathbf{x}} = (0,0,0)$ and vertices $\hat{\mathbf{x}}_{1,0,s}$, $\hat{\mathbf{x}}_{-1,0,s}$, $\hat{\mathbf{x}}_{0,1,s}$, $\hat{\mathbf{x}}_{0,-1,s}$, $\hat{\mathbf{x}}_{1,1,s}$, $\hat{\mathbf{x}}_{-1,-1,s}$ with $s = -1, 0, 1$, we define an affine transformation $\mathscr{H}_P$ such that $\mathbf{x} = \mathscr{H}_P(\hat{\mathbf{x}}) = \mathscr{D}_P \hat{\mathbf{x}} + d_P$, yielding $\mathscr{H}_P(\hat{\mathbf{x}}_{k,l}) = \mathbf{x}_{n+k,m+l}$. This affine transformation can be simply defined as follows:

$$\mathscr{D}_P = \begin{bmatrix} x_{n+1,m,p} - x_{n,m,p} & x_{n+1,m+1,p} - x_{n+1,m,p} & x_{n+1,m+1,p+1} - x_{n+1,m+1,p} \\ y_{n+1,m,p} - y_{n,m,p} & y_{n+1,m+1,p} - y_{n+1,m,p} & y_{n+1,m+1,p+1} - y_{n+1,m+1,p} \\ z_{n+1,m,p} - z_{n,m,p} & z_{n+1,m+1,p} - y_{n+1,m,p} & z_{n+1,m+1,p+1} - z_{n+1,m+1,p} \end{bmatrix},$$

and $d_P = \begin{bmatrix} x_{n,m,p} & y_{n,m,p} & z_{n,m,p} \end{bmatrix}^t$, where $(x_{u,v,s}, y_{u,v,s}, z_{u,v,s})$ are the coordinates of the nodes $\mathbf{x}_{u,v,s}$. The degree of freedom and basis functions on the reference hexagonal prism $\hat{P}$ can be translate to the degree of freedom and basis functions on the arbitrary hexagonal prism P. In particular, we have

$$\hat{\phi}_{n,m,k} = \phi_{n,m,k} \circ \mathscr{H}_P \qquad \nabla\hat{\phi}_{n,m,k} = \mathscr{D}_P^t \nabla\phi_{n,m,k} \circ \mathscr{H}_P.$$

consider the following stencil for the stiffness matrix

$$A_h = |\det \mathscr{D}_P| \left[\begin{bmatrix} & a_{0,1,-1} & a_{1,1,-1} \\ a_{-1,0,-1} & a_{0,0,-1} & a_{1,0,-1} \\ a_{-1,-1,-1} & a_{0,-1,-1} & \end{bmatrix} \begin{bmatrix} & a_{0,1,0} & a_{1,1,0} \\ a_{-1,0,0} & a_{0,0,0} & a_{1,0,0} \\ a_{-1,-1,0} & a_{0,-1,0} & \end{bmatrix} \begin{bmatrix} & a_{0,1,1} & a_{1,1,1} \\ a_{-1,0,1} & a_{0,0,1} & a_{1,0,1} \\ a_{-1,-1,1} & a_{0,-1,1} & \end{bmatrix} \right],$$

By using the change of variable associated with the affine mapping $\mathscr{H}_P$, we obtain the following expressions for the stiffness stencil elements:

$$\begin{aligned}
a_{0,1,-1} &= \int_{\hat{P}_8} (\mathscr{D}_P^{-1})^t \nabla\hat{\phi}_{0,1,-1} \cdot (\mathscr{D}_P^{-1})^t \nabla\hat{\phi}_{0,0,0} d\hat{\mathbf{x}} + \int_{\hat{P}_9} (\mathscr{D}_P^{-1})^t \nabla\hat{\phi}_{0,1,-1} \cdot (\mathscr{D}_P^{-1})^t \nabla\hat{\phi}_{0,0,0} d\hat{\mathbf{x}}, \\
a_{1,1,-1} &= \int_{\hat{P}_7} (\mathscr{D}_P^{-1})^t \nabla\hat{\phi}_{1,1,-1} \cdot (\mathscr{D}_P^{-1})^t \nabla\hat{\phi}_{0,0,0} d\hat{\mathbf{x}} + \int_{\hat{P}_8} (\mathscr{D}_P^{-1})^t \nabla\hat{\phi}_{1,1,-1} \cdot (\mathscr{D}_P^{-1})^t \nabla\hat{\phi}_{0,0,0} d\hat{\mathbf{x}}, \\
a_{-1,0,-1} &= \int_{\hat{P}_9} (\mathscr{D}_P^{-1})^t \nabla\hat{\phi}_{-1,0,-1} \cdot (\mathscr{D}_P^{-1})^t \nabla\hat{\phi}_{0,0,0} d\hat{\mathbf{x}} + \int_{\hat{P}_{10}} (\mathscr{D}_P^{-1})^t \nabla\hat{\phi}_{-1,0,-1} \cdot (\mathscr{D}_P^{-1})^t \nabla\hat{\phi}_{0,0,0} d\hat{\mathbf{x}}, \\
a_{0,0,-1} &= \sum_{i=5}^{12} \int_{\hat{T}_i} (\mathscr{D}_P^{-1})^t \nabla\hat{\phi}_{0,0,-1} \cdot (\mathscr{D}_P^{-1})^t \nabla\hat{\phi}_{0,0,0} d\hat{\mathbf{x}}, \\
a_{1,0,-1} &= \int_{\hat{P}_5} (\mathscr{D}_P^{-1})^t \nabla\hat{\phi}_{1,0,-1} \cdot (\mathscr{D}_P^{-1})^t \nabla\hat{\phi}_{0,0,0} d\hat{\mathbf{x}} + \int_{\hat{P}_{12}} (\mathscr{D}_P^{-1})^t \nabla\hat{\phi}_{1,0,-1} \cdot (\mathscr{D}_P^{-1})^t \nabla\hat{\phi}_{0,0,0} d\hat{\mathbf{x}}, \\
a_{-1,-1,-1} &= \int_{\hat{P}_{10}} (\mathscr{D}_P^{-1})^t \nabla\hat{\phi}_{-1,-1,-1} \cdot (\mathscr{D}_P^{-1})^t \nabla\hat{\phi}_{0,0,0} d\hat{\mathbf{x}} + \int_{\hat{P}_{11}} (\mathscr{D}_P^{-1})^t \nabla\hat{\phi}_{-1,-1,-1} \cdot (\mathscr{D}_P^{-1})^t \nabla\hat{\phi}_{0,0,0} d\hat{\mathbf{x}}, \\
a_{0,-1,-1} &= \int_{\hat{P}_{11}} (\mathscr{D}_P^{-1})^t \nabla\hat{\phi}_{0,-1,-1} \cdot (\mathscr{D}_P^{-1})^t \nabla\hat{\phi}_{0,0,0} d\hat{\mathbf{x}} + \int_{\hat{P}_{12}} (\mathscr{D}_P^{-1})^t \nabla\hat{\phi}_{0,-1,-1} \cdot (\mathscr{D}_P^{-1})^t \nabla\hat{\phi}_{0,0,0} d\hat{\mathbf{x}}, \\
a_{0,1,0} &= \int_{\hat{P}_8} (\mathscr{D}_P^{-1})^t \nabla\hat{\phi}_{0,1,,0} \cdot (\mathscr{D}_P^{-1})^t \nabla\hat{\phi}_{0,0,0} d\hat{\mathbf{x}} + \int_{\hat{P}_9} (\mathscr{D}_P^{-1})^t \nabla\hat{\phi}_{0,1,0} \cdot (\mathscr{D}_P^{-1})^t \nabla\hat{\phi}_{0,0,0} d\hat{\mathbf{x}}, \\
a_{1,1,0} &= \int_{\hat{P}_7} (\mathscr{D}_P^{-1})^t \nabla\hat{\phi}_{1,1,0} \cdot (\mathscr{D}_P^{-1})^t \nabla\hat{\phi}_{0,0,0} d\hat{\mathbf{x}} + \int_{\hat{P}_8} (\mathscr{D}_P^{-1})^t \nabla\hat{\phi}_{1,1,0} \cdot (\mathscr{D}_P^{-1})^t \nabla\hat{\phi}_{0,0,0} d\hat{\mathbf{x}}, \\
a_{-1,0,0} &= \int_{\hat{P}_9} (\mathscr{D}_P^{-1})^t \nabla\hat{\phi}_{-1,0,0} \cdot (\mathscr{D}_P^{-1})^t \nabla\hat{\phi}_{0,0,0} d\hat{\mathbf{x}} + \int_{\hat{P}_{10}} (\mathscr{D}_P^{-1})^t \nabla\hat{\phi}_{-1,0,0} \cdot (\mathscr{D}_P^{-1})^t \nabla\hat{\phi}_{0,0,0} d\hat{\mathbf{x}}, \\
a_{0,0,0} &= \sum_{i=1}^{12} \int_{\hat{T}_i} (\mathscr{D}_P^{-1})^t \nabla\hat{\phi}_{0,0,0} \cdot (\mathscr{D}_P^{-1})^t \nabla\hat{\phi}_{0,0,0} d\hat{\mathbf{x}}, \\
a_{1,0,0} &= \int_{\hat{P}_5} (\mathscr{D}_P^{-1})^t \nabla\hat{\phi}_{1,0,0} \cdot (\mathscr{D}_P^{-1})^t \nabla\hat{\phi}_{0,0,0} d\hat{\mathbf{x}} + \int_{\hat{P}_{12}} (\mathscr{D}_P^{-1})^t \nabla\hat{\phi}_{1,0,0} \cdot (\mathscr{D}_P^{-1})^t \nabla\hat{\phi}_{0,0,0} d\hat{\mathbf{x}}, \\
a_{-1,-1,0} &= \int_{\hat{P}_{10}} (\mathscr{D}_P^{-1})^t \nabla\hat{\phi}_{-1,-1,0} \cdot (\mathscr{D}_P^{-1})^t \nabla\hat{\phi}_{0,0,0} d\hat{\mathbf{x}} + \int_{\hat{P}_{11}} (\mathscr{D}_P^{-1})^t \nabla\hat{\phi}_{-1,-1,0} \cdot (\mathscr{D}_P^{-1})^t \nabla\hat{\phi}_{0,0,0} d\hat{\mathbf{x}}, \\
a_{0,-1,0} &= \int_{\hat{P}_{11}} (\mathscr{D}_P^{-1})^t \nabla\hat{\phi}_{0,-1,0} \cdot (\mathscr{D}_P^{-1})^t \nabla\hat{\phi}_{0,0,0} d\hat{\mathbf{x}} + \int_{\hat{P}_{12}} (\mathscr{D}_P^{-1})^t \nabla\hat{\phi}_{0,-1,0} \cdot (\mathscr{D}_P^{-1})^t \nabla\hat{\phi}_{0,0,0} d\hat{\mathbf{x}},
\end{aligned}$$

$$
\begin{aligned}
a_{0,1,1} &= \int_{\hat{P}_8} (\mathscr{D}_P^{-1})^t \nabla\hat{\phi}_{0,1,1} \cdot (\mathscr{D}_P^{-1})^t \nabla\hat{\phi}_{0,0,0} d\hat{\mathbf{x}} + \int_{\hat{P}_9} (\mathscr{D}_P^{-1})^t \nabla\hat{\phi}_{0,1,1} \cdot (\mathscr{D}_P^{-1})^t \nabla\hat{\phi}_{0,0,0} d\hat{\mathbf{x}},\\
a_{1,1,1} &= \int_{\hat{P}_7} (\mathscr{D}_P^{-1})^t \nabla\hat{\phi}_{1,1,1} \cdot (\mathscr{D}_P^{-1})^t \nabla\hat{\phi}_{0,0,0} d\hat{\mathbf{x}} + \int_{\hat{P}_8} (\mathscr{D}_P^{-1})^t \nabla\hat{\phi}_{1,1,1} \cdot (\mathscr{D}_P^{-1})^t \nabla\hat{\phi}_{0,0,0} d\hat{\mathbf{x}},\\
a_{-1,0,1} &= \int_{\hat{P}_9} (\mathscr{D}_P^{-1})^t \nabla\hat{\phi}_{-1,0,1} \cdot (\mathscr{D}_P^{-1})^t \nabla\hat{\phi}_{0,0,0} d\hat{\mathbf{x}} + \int_{\hat{P}_{10}} (\mathscr{D}_P^{-1})^t \nabla\hat{\phi}_{-1,0,1} \cdot (\mathscr{D}_P^{-1})^t \nabla\hat{\phi}_{0,0,0} d\hat{\mathbf{x}},\\
a_{0,0,1} &= \sum_{i=5}^{12} \int_{\hat{T}_i} (\mathscr{D}_P^{-1})^t \nabla\hat{\phi}_{0,0,1} \cdot (\mathscr{D}_P^{-1})^t \nabla\hat{\phi}_{0,0,0} d\hat{\mathbf{x}},\\
a_{1,0,1} &= \int_{\hat{P}_5} (\mathscr{D}_P^{-1})^t \nabla\hat{\phi}_{1,0,1} \cdot (\mathscr{D}_P^{-1})^t \nabla\hat{\phi}_{0,0,0} d\hat{\mathbf{x}} + \int_{\hat{P}_{12}} (\mathscr{D}_P^{-1})^t \nabla\hat{\phi}_{1,0,1} \cdot (\mathscr{D}_P^{-1})^t \nabla\hat{\phi}_{0,0,0} d\hat{\mathbf{x}},\\
a_{-1,-1,1} &= \int_{\hat{P}_{10}} (\mathscr{D}_P^{-1})^t \nabla\hat{\phi}_{-1,-1,1} \cdot (\mathscr{D}_P^{-1})^t \nabla\hat{\phi}_{0,0,0} d\hat{\mathbf{x}} + \int_{\hat{P}_{11}} (\mathscr{D}_P^{-1})^t \nabla\hat{\phi}_{-1,-1,1} \cdot (\mathscr{D}_P^{-1})^t \nabla\hat{\phi}_{0,0,0} d\hat{\mathbf{x}},\\
a_{0,-1,1} &= \int_{\hat{P}_{11}} (\mathscr{D}_P^{-1})^t \nabla\hat{\phi}_{0,-1,1} \cdot (\mathscr{D}_P^{-1})^t \nabla\hat{\phi}_{0,0,0} d\hat{\mathbf{x}} + \int_{\hat{P}_{12}} (\mathscr{D}_P^{-1})^t \nabla\hat{\phi}_{0,-1,1} \cdot (\mathscr{D}_P^{-1})^t \nabla\hat{\phi}_{0,0,0} d\hat{\mathbf{x}}.
\end{aligned}
$$

Using C_H as follows,

$$
C_H = \mathscr{D}_P^{-1}(\mathscr{D}_P^{-1})^T = \begin{bmatrix} c_{11} & c_{12} & c_{13} \\ c_{21} & c_{22} & c_{23} \\ c_{31} & c_{32} & c_{33} \end{bmatrix},
$$

we can simply compute the elements of A_h from the following expression:

$$
A_h = |\det \mathscr{D}_P| = (c_{11}A_{xx} + 2c_{12}A_{xy} + c_{22}A_{yy} + c_{33}A_{zz}).
$$

Here, we have

$$
\begin{aligned}
A_{xx} &= \left[\begin{bmatrix} 0 & 0 & 0 \\ \frac{-2}{12} & \frac{4}{12} & \frac{-2}{12} \\ 0 & 0 & 0 \end{bmatrix} \begin{bmatrix} 0 & 0 & 0 \\ \frac{-4}{6} & \frac{8}{6} & \frac{-4}{6} \\ 0 & 0 & 0 \end{bmatrix} \begin{bmatrix} 0 & 0 & 0 \\ \frac{-2}{12} & \frac{4}{12} & \frac{-2}{12} \\ 0 & 0 & 0 \end{bmatrix} \right],\\
A_{yy} &= \left[\begin{bmatrix} 0 & \frac{-2}{12} & 0 \\ 0 & \frac{4}{12} & 0 \\ 0 & \frac{-2}{12} & 0 \end{bmatrix} \begin{bmatrix} 0 & \frac{-4}{6} & 0 \\ 0 & \frac{8}{6} & 0 \\ 0 & \frac{-4}{6} & 0 \end{bmatrix} \begin{bmatrix} 0 & \frac{-2}{12} & 0 \\ 0 & \frac{4}{12} & 0 \\ 0 & \frac{-2}{12} & 0 \end{bmatrix} \right],\\
A_{xz} &= \left[\begin{bmatrix} 0 & \frac{1}{12} & \frac{-1}{12} \\ \frac{-2}{12} & 0 & \frac{-2}{12} \\ \frac{-1}{12} & \frac{1}{12} & 0 \end{bmatrix} \begin{bmatrix} 0 & 0 & 0 \\ 0 & 0 & 0 \\ 0 & 0 & 0 \end{bmatrix} \begin{bmatrix} 0 & \frac{1}{12} & \frac{-1}{12} \\ \frac{-2}{12} & 0 & \frac{-2}{12} \\ \frac{-1}{12} & \frac{1}{12} & 0 \end{bmatrix} \right],\\
A_{yz} &= \left[\begin{bmatrix} 0 & \frac{-2}{12} & \frac{-1}{12} \\ \frac{1}{12} & 0 & \frac{1}{12} \\ \frac{-1}{12} & \frac{-2}{12} & 0 \end{bmatrix} \begin{bmatrix} 0 & 0 & 0 \\ 0 & 0 & 0 \\ 0 & 0 & 0 \end{bmatrix} \begin{bmatrix} 0 & \frac{-2}{12} & \frac{-1}{12} \\ \frac{1}{12} & 0 & \frac{1}{12} \\ \frac{-1}{12} & \frac{-2}{12} & 0 \end{bmatrix} \right],\\
A_{xy} &= \left[\begin{bmatrix} 0 & \frac{1}{12} & \frac{-1}{12} \\ \frac{1}{12} & \frac{-2}{12} & \frac{1}{12} \\ \frac{-1}{12} & \frac{1}{12} & 0 \end{bmatrix} \begin{bmatrix} 0 & \frac{2}{6} & \frac{-2}{6} \\ \frac{2}{6} & \frac{-4}{6} & \frac{2}{6} \\ \frac{-2}{6} & \frac{2}{6} & 0 \end{bmatrix} \begin{bmatrix} 0 & \frac{1}{12} & \frac{-1}{12} \\ \frac{1}{12} & \frac{-2}{12} & \frac{1}{12} \\ \frac{-1}{12} & \frac{1}{12} & 0 \end{bmatrix} \right],\\
A_{zz} &= \left[\begin{bmatrix} 0 & \frac{-1}{12} & \frac{-1}{12} \\ \frac{-1}{12} & \frac{-6}{12} & \frac{-1}{12} \\ \frac{-1}{12} & \frac{-1}{12} & 0 \end{bmatrix} \begin{bmatrix} 0 & \frac{2}{12} & \frac{2}{12} \\ \frac{2}{12} & 1 & \frac{2}{12} \\ \frac{2}{12} & \frac{2}{12} & 0 \end{bmatrix} \begin{bmatrix} 0 & \frac{-1}{12} & \frac{-1}{12} \\ \frac{-1}{12} & \frac{-6}{12} & \frac{-1}{12} \\ \frac{-1}{12} & \frac{-1}{12} & 0 \end{bmatrix} \right],
\end{aligned}
$$

considering the coordinates in terms of the geometric parameters, $0 < \alpha, \beta < \pi/2$, we can compute the elements of C_H then the A_h stencil as follows:

$$C_H = \frac{1}{h^2}\begin{bmatrix} 1+\cot^2\beta & \cot\beta\cot\alpha+\cot^2\beta & 0 \\ \cot\beta\cot\alpha+\cot^2\beta & (\cot\alpha+\cot\beta)^2 & 0 \\ 0 & 0 & 1 \end{bmatrix}.$$

Also, we have

$$\begin{aligned}
&a_{0,1,-1} = a_{0,-1,-1} = a_{0,1,1} = a_{0,-1,1} = \frac{1}{12h^2}\left(-2\cot^2\alpha - 2\cot\alpha\cot\beta - 1\right), \\
&a_{1,0,-1} = a_{-1,0,-1} = a_{1,0,1} = a_{-1,0,1} = \frac{1}{12h^2}\left(2\cot\alpha\cot\beta - 3\right), \\
&a_{1,1,-1} = a_{-1,-1,-1} = a_{1,1,1} = a_{-1,-1,1} = \frac{1}{12h^2}\left(-2\cot^2\beta - 2\cot\alpha\cot\beta - 1\right), \\
&a_{0,0,-1} = a_{0,0,1} = \frac{1}{12h^2}\left(4(\cot\alpha+\cot\beta)^2 - 4\cot\alpha\cot\beta - 2\right), \\
&a_{0,1,0} = a_{0,-1,0} = \frac{1}{6h^2}\left(1 - 4\cot^2\alpha - 4\cot\alpha\cot\beta\right), \\
&a_{1,0,0} = a_{-1,0,0} = \frac{1}{6h^2}\left(4\cot\alpha\cot\beta - 3\right), \\
&a_{1,1,0} = a_{-1,-1,0} = \frac{1}{6h^2}\left(1 - 4\cot^2\beta - 4\cot\alpha\cot\beta\right), \\
&a_{0,0,0} = \frac{1}{6h^2}\left(8(\cot\alpha+\cot\beta)^2 - 8\cot\alpha\cot\beta + 14\right),
\end{aligned} \tag{15}$$

where all the above coefficients are normalized by $|\det\mathscr{D}_P|$.

In the special limit case $\beta = \pi/2$, the stiffness stencil is calculated to be

$$A = \frac{1}{24h^2}\left[\begin{bmatrix} & -6 & -2 \\ -6 & 4 & -6 \\ -2 & -6 & \end{bmatrix}\begin{bmatrix} & -12 & 4 \\ -12 & 88 & -12 \\ 4 & -12 & \end{bmatrix}\begin{bmatrix} & -6 & -2 \\ -6 & 4 & -6 \\ -2 & -6 & \end{bmatrix}\right].$$

Moreover, the stencil form corresponding to the mass matrix, B_h, is fixed on every triangular prism element that is

$$B_h = \frac{1}{72}\left[\begin{bmatrix} & 1 & 1 \\ 1 & 6 & 1 \\ 1 & 1 & \end{bmatrix}\begin{bmatrix} & 4 & 4 \\ 4 & 24 & 4 \\ 4 & 4 & \end{bmatrix}\begin{bmatrix} & 1 & 1 \\ 1 & 6 & 1 \\ 1 & 1 & \end{bmatrix}\right].$$

To apply the presented analysis we also need to define the components of the multigrid waveform relaxation method. Regarding the intergrid transfer operators, the stencil of the restriction operator, I_h^{2h}, is given by

$$I_h^{2h} = \frac{1}{32}\left[\begin{bmatrix} & 1 & 1 \\ 1 & 2 & 1 \\ 1 & 1 & \end{bmatrix}\begin{bmatrix} & 2 & 2 \\ 2 & 4 & 2 \\ 2 & 2 & \end{bmatrix}\begin{bmatrix} & 1 & 1 \\ 1 & 2 & 1 \\ 1 & 1 & \end{bmatrix}\right].$$

So, we can obtain its fourier representation as follows

$$\widehat{I}_h^{2h}(\boldsymbol{\theta}^\alpha) = \frac{1}{4}\left(1+\cos(\theta_1^\alpha)\right)\left(1+\cos(\theta_2^\alpha)\right) \quad \text{s.t} \quad \boldsymbol{\theta}^\alpha = (\theta_1^\alpha, \theta_2^\alpha).$$

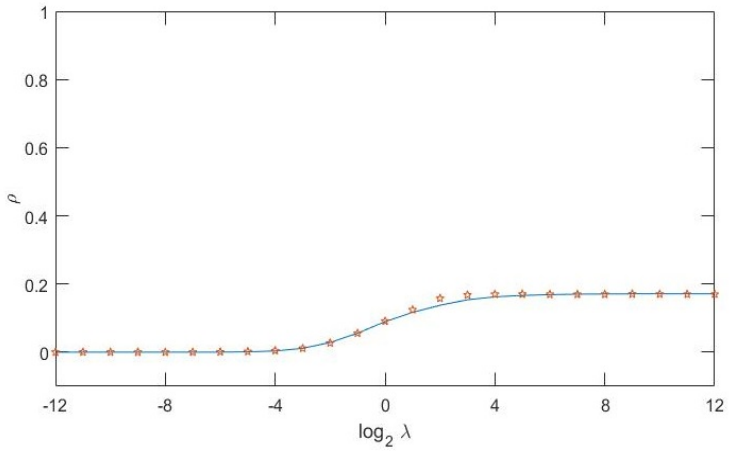

Figure 8: Two-grid convergence factor predicted by analysis and the experimentally convergence factor computed by w(1-1)-cycle for various parameters λ ranging from 2^{-12} to 2^{12} on triangular prism element with angles $\alpha = 45, \beta = 90$.

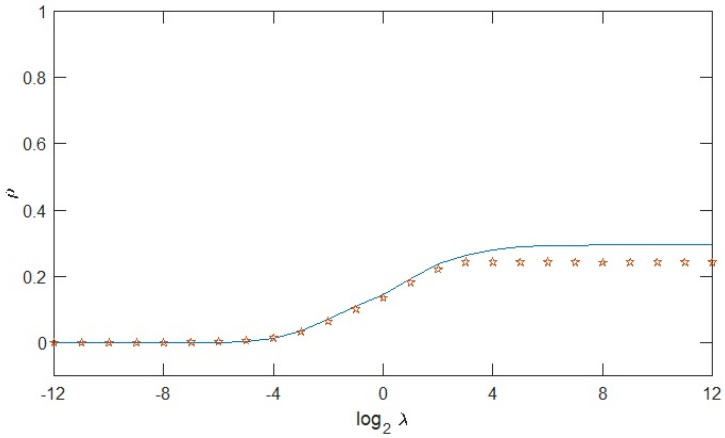

Figure 9: Two-grid convergence factor predicted by analysis and the experimentally convergence factor computed by w(1-1)-cycle for various parameters λ ranging from 2^{-12} to 2^{12} on triangular prism element with angles $\alpha = 40, \beta = 50$.

The prolongation operator I_{2h}^{h}, is obtained according to the relation $I_{h}^{2h} = \frac{1}{8} I_{2h}^{h}$.

Numerical results depending on the parameter $\lambda = \tau/h^2$, ranging from 2^{-12} to 2^{12}, comparing the two-grid convergence factors predicted by SAMA together with the asymptotic convergence rates obtained by using W-cycle multigrid waveform relaxation considering several values for α and β, "$\alpha = 45^\circ \beta = 90^\circ$", "$\alpha = 40^\circ \beta = 50^\circ$", "$\alpha = 50^\circ \beta = 70^\circ$", "$\alpha = 60^\circ \beta = 60^\circ$" and "$\alpha = 80^\circ \beta = 40^\circ$", are illustrated respectively in Figures 8, 9, 10, 11, 12. In this Figure, two smoothing steps are considered and the number of time steps is set 32 ($M = 32$). Moreover, the multigrid waveform relaxation results are calculated by considering a random initial guess and a zero right-hand side. As we can see, the analysis

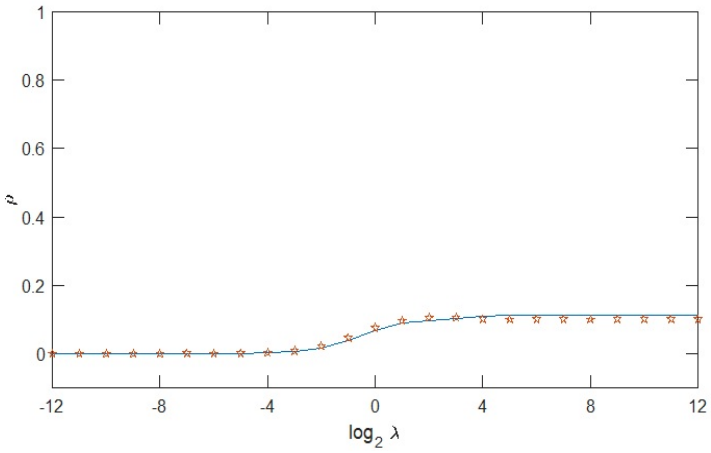

Figure 10: Two-grid convergence factor predicted by analysis and the experimentally convergence factor computed by w(1-1)-cycle for various parameters λ ranging from 2^{-12} to 2^{12} on triangular prism element with angles $\alpha = 50, \beta = 70$.

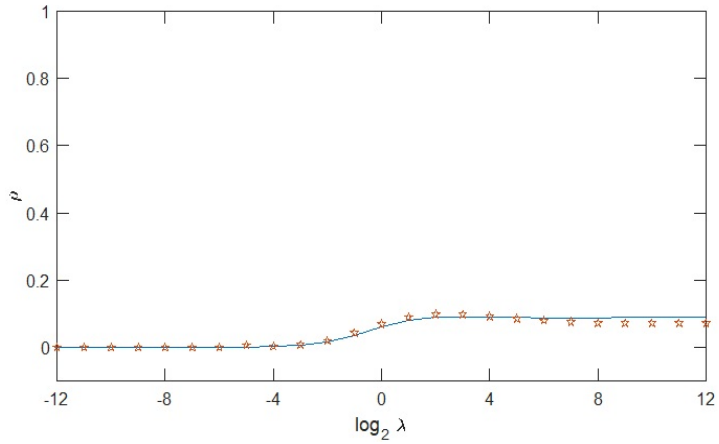

Figure 11: Two-grid convergence factor predicted by analysis and the experimentally convergence factor computed by w(1-1)-cycle for various parameters λ ranging from 2^{-12} to 2^{12} on triangular prism element with angles $\alpha = 60, \beta = 60$.

results of SAMA and the rates experimentally computed match very accurate. In Figures 9-12, you can also see that the convergence factors depend on the angles of the coarsest triangles, i.e. better convergence factors are obtain for equilateral triangle and its values become worse when one of the angles tends to be small.

Also in the third row of Table 2 , the asymptotic convergence factor computed by W(1,1) cycle together with their predicted results by SAMA (in parentheses) are displayed for different values of τ and a fixed grid size $64 \times 64 \times 32$, where $\beta = 90^\circ$. We can observe an accurate match between the experimental and the predicted results. In the fourth row of Table 1 we substitute the matrix B_h by the

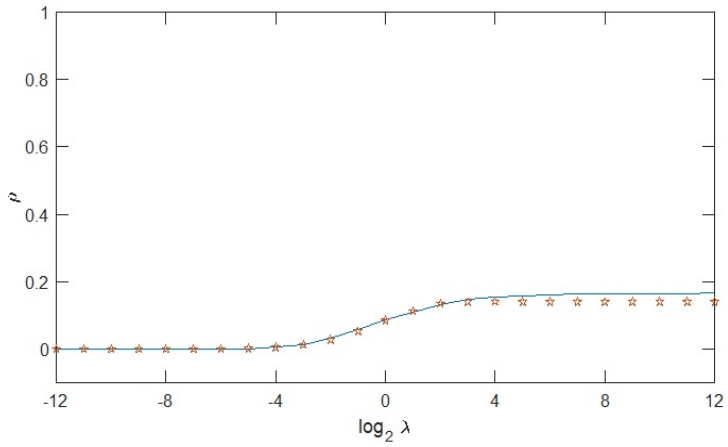

Figure 12: Two-grid convergence factor predicted by analysis and the experimentally convergence factor computed by w(1-1)-cycle for various parameters λ ranging from 2^{-12} to 2^{12} on triangular prism element with angles $\alpha = 80, \beta = 40$.

identity matrix. One can see that the results when choosing B_h as the identity matrix match with the case in which the applied discretization method is the finite difference scheme.

4 Conclusions

In this work, we presented the two-grid SAMA analysis for predicting the convergence factor of a multigrid waveform relaxation method for finite element discretization in two and three spatial dimensions. The Crank-Nicolson discretization in time and the rectangular and triangular grid in two dimensions and their extensions to cubic and general triangular prism meshes in three dimensions, for the spatial discretization, are considered respectively. The computations corresponding to the general triangular prism element were new and the influence of angles in a prism element was illustrated by presenting several examples. The proposed SAMA analysis allows us to systematically study the behavior of the multigrid waveform relaxation method for finite element discretizations for different spatial meshes. Moreover, in this work, we showed the finite element discretization is more general than that for finite difference discretization, since the results when matrix B_h is the identity matrix, are comparable with the case in which a finite difference discretization method is applied. Our work was a general discussion on some famous equations. So, the eager reader could refer for example to the works [7, 9] to see more about the benefits of this analysis.

References

[1] C. Engwer, R.D. Falgout, U.M. Yang, *Stencil computations for PDE-based applications with examples from DUNE and hypre*, Concurr. Comput. Pract. Exp **29** (2017) e4097.

[2] S. Friedhoff, S. MacLachlan, *A generalized predictive analysis tool for multigrid methods*, Numer. Linear Algebra Appl. **22** (2015) 618–647.

[3] M.J. Gander, *50 Years of Time Parallel Time Integration*, Springer, (2015) 69–113.

[4] F.J. Gaspar, J.L. Gracia, F.J. Lisbona, *Fourier analysis for multigrid methods on triangular grids*, SIAM J. Sci. Comput. **31** (2009) 2081–2102.

[5] F.J. Gaspar, C. Rodrigo, *Multigrid waveform relaxation for the time-fractional heat equation*, SIAM J. Sci. Comput. **39** (2017) A1201–A1224.

[6] M.S. Gockenbach, *Understanding and Implementing the Finite Element Method*, SIAM, 2006.

[7] X. Hu, C. Rodrigo, F.J. Gaspar, *Using hierarchical matrices in the solution of the time-fractional heat equation by multigrid waveform relaxation.*, J. Comput. Phys. **416** (2020) 109540.

[8] Ch. Lubich, A. Ostermann, *Multi-grid dynamic iteration for parabolic equations*, BIT Numer. Math. **27** (1987) 216–234.

[9] M.F. Malacarne, M.A. Villela Pinto, S.R. Franco, *Subdomain Method in Time with Waveform Relaxation in Space Applied to the Wave Equation Combined with the Multigrid Method*, Available at SSRN 4089078 (2022).

[10] U. Miekkala, O. Nevanlinna, *Convergence of dynamic iteration methods for initial value problems*, SIAM J. Sci. Statist. Comput. **8** (1987) 459–482.

[11] C. Rodrigo,F.J. Gaspar, F.J. Lisbona, *Geometric multigrid methods on semi-structured triangular grids*, The 7 th GRACM Congress hosts the 1 st ECCOMAS PhD Olympiad (2011) P.175.

[12] U. Trottenberg,C.W. Oosterlee, A. Schuller, *Multigrid*, Elsevier, 2000.

[13] S. Vandewalle, D. Roose, *The parallel waveform relaxation multigrid method*, Parallel Processing for Scientific Computing (1989) 152–156.

[14] R. Wienands, W. Joppich, *Practical Fourier Analysis for Multigrid Methods*, Chapman and Hall/CRC, 2004.